



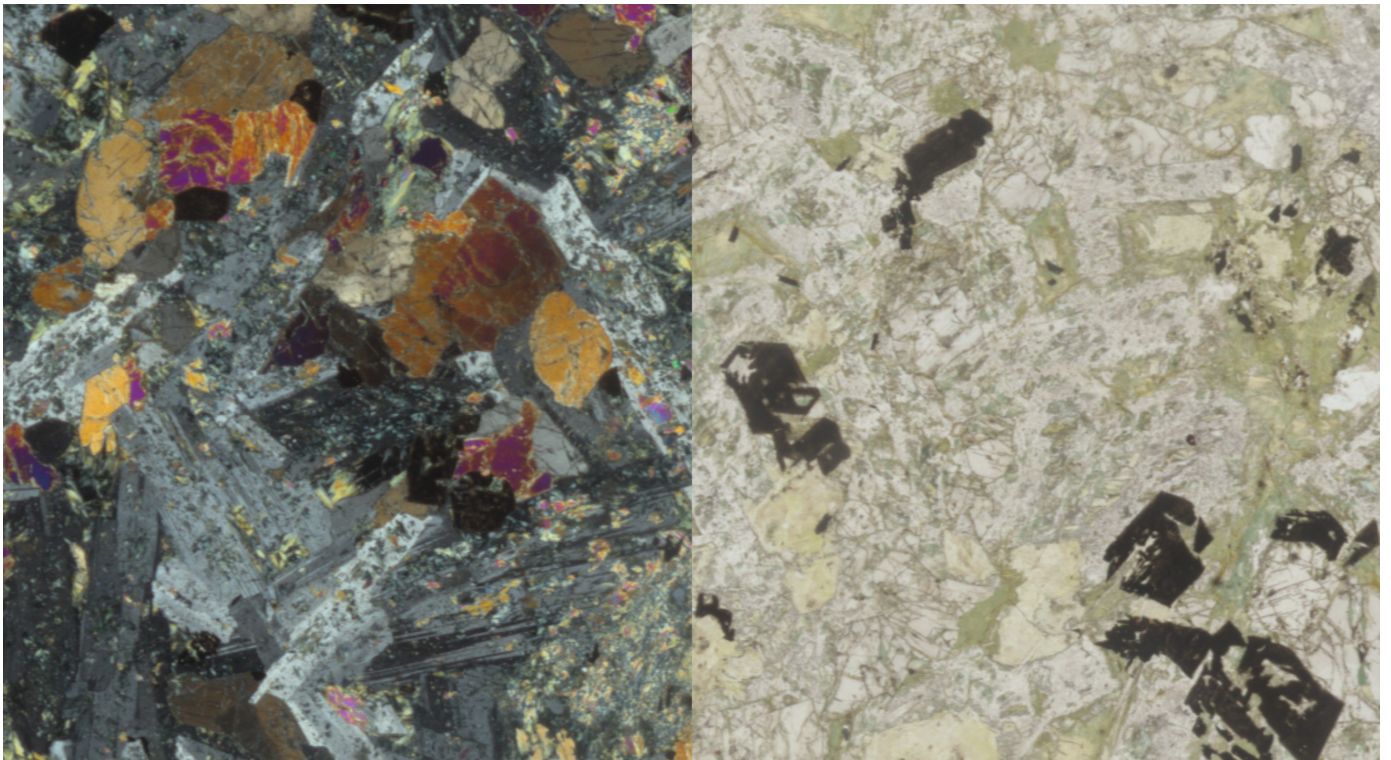
Stockholm  
University

# Bachelor Thesis

Degree Project in  
Geology 15 hp

## **A Petrographic and Geochemical Study on the Tectonic Origin of the Bourne Complex, Ellesmere Island, Arctic Canada**

Mahmud Tahir Erdogan



Stockholm 2024

Department of Geological Sciences  
Stockholm University  
SE-106 91 Stockholm

## *Abstract*

The Bourne Complex, situated in Ellesmere Island, Arctic Canada, has remained unresearched for the past few decades, with the last geochemical study conducted over 30 years ago that claimed a subduction-related tectonic origin. This study aims to revisit and expand upon previous analyses using a set of collected samples. Ten samples were petrographically and geochemically analysed. The rocks were classified, magmatic relationships were established, and trace element analysis was conducted to establish a tectonic setting. The samples show trace element characteristics indicative of both convergent and divergent tectonic settings but lack subduction-related characteristics, indicating a non-subduction-related origin. The samples more closely resemble basalts originating from continental intraplate settings. Further studies using more samples and utilizing isotopic data and geochronological dating are needed to determine the tectonic evolution of the Bourne Complex.

## Table of Contents

1 - Introduction.....	1
2 – Geological background .....	3
2.1 – Northern Ellesmere Island.....	3
2.2 – Bourne Complex .....	3
3 – Methods.....	5
4.1 – Hand sample & Petrographic analysis.....	7
4.1.1 - Hand sample.....	7
4.1.2 - Petrographic Analysis .....	7
4.1.3 - Geochemical analysis.....	10
5 - Discussion .....	13
5.1 – Selection of diagrams, metamorphic alteration and element mobility .....	13
5.2 – Cogenetic magma series.....	14
Conclusion.....	21
Acknowledgements .....	22
References .....	23
Appendix A – Abbreviations.....	26
Appendix B – Point counting grid example .....	27
Appendix C – Point counting results.....	28
Appendix D – Petrographic Analysis.....	33
VP17-41 .....	33
VP17-43 .....	33
VP17-44 .....	34
VP17-51 .....	35
VP17-52 .....	35
VP17-53 .....	36
VP17-55 .....	37
VP17-56 .....	37
VP17-57 .....	38
VP17-59 .....	39
Appendix E – Alteration ratio .....	40
Appendix F – IUGS modal classification .....	41



## **1 - Introduction**

Ellesmere Island is the most northern island in the Canadian Arctic Archipelago, situated in Nunavut, Arctic Canada and bordered by Axel Heiberg Island, Devon Island and Greenland on its western, southern and eastern side respectively (Figure 1). Parts of the island have been extensively studied since its first expedition by the Geological Survey of Canada in 1953 (Trettin et al. 1998), and research is still ongoing, rapidly changing what we know about the island's history and formation (e.g Koch et al. 2022; Faehnrich et al. 2023). However, the Bourne Complex, located on the far northwestern corner of the Island, has remained largely untouched and unresearched.

Existing knowledge of the Bourne Complex is limited due to the structural complexity and remoteness of the region, with poor exposure and an abundance of intrusions (Trettin et al. 1998). Previously conducted studies have been limited and primarily focused on establishing field relationships. Some geochemical analyses were carried out by Henry (1991), who classified the samples as subalkaline and alkaline andesites and basalts and interpreted them as related to a subduction-to-back-arc related tectonic setting.

This study aims to expand on Henry's earlier work by conducting petrographic and whole-rock geochemical analysis on new samples from the Bourne Complex; these will build on Henry's work and place the samples within a broader geological context. The purpose is to analyse and classify the samples and determine a tectonic setting through petrographical and geochemical methods. Analytical methods include rock classification, identification of possible cogenetic magma series and tectonic discrimination diagrams.

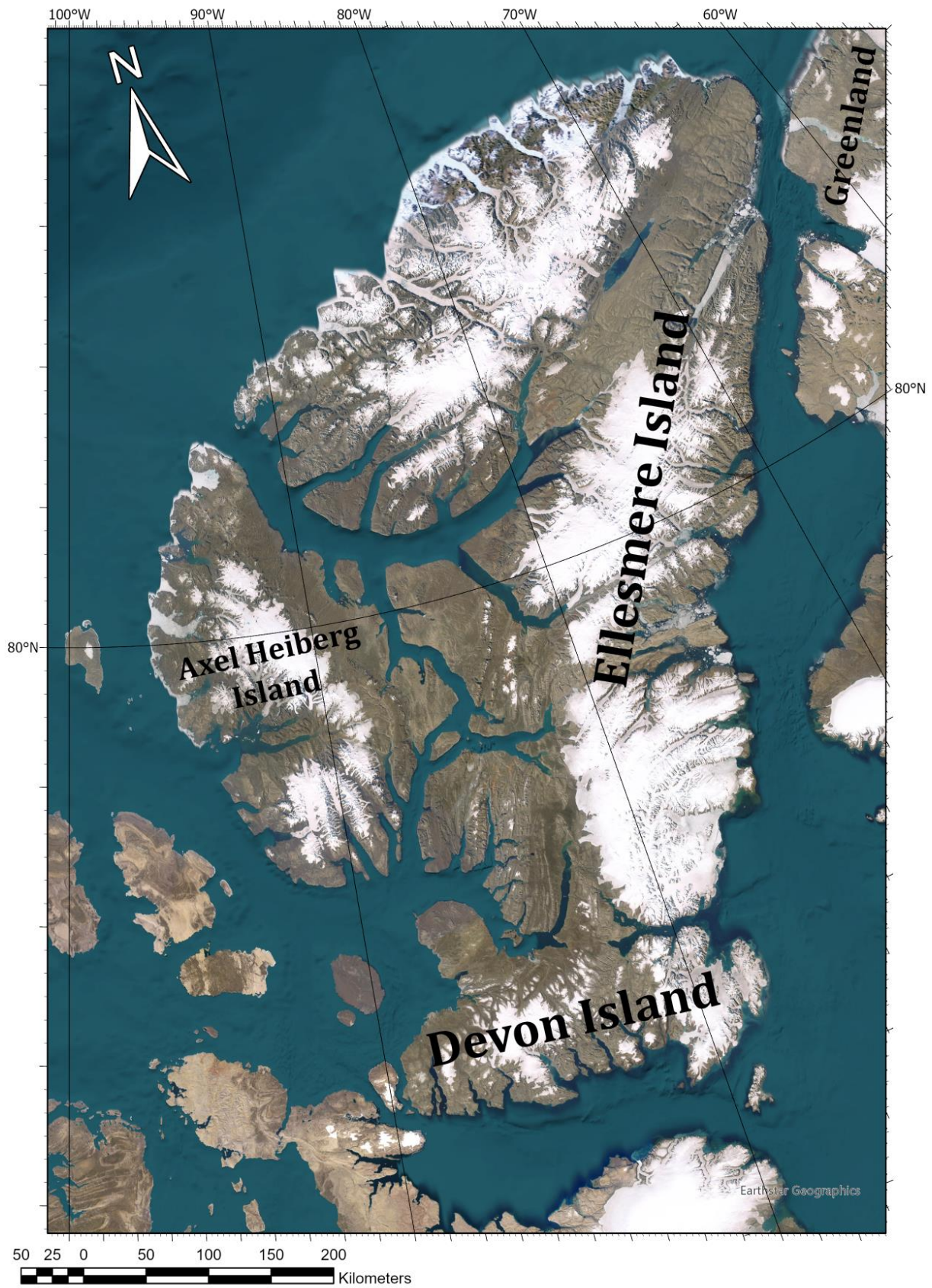


Figure 1: Satellite map of Ellesmere Island and adjacent Islands. Modified from Esri (2024).

## **2 – Geological background**

### ***2.1 – Northern Ellesmere Island***

Northern Ellesmere Island consists of four major structural units (Figure 2): the Canadian Shield, the Franklinian Mobile Belt, the Sverdrup Basin, and the Pearya Terrane. The Canadian shield lies exposed only on south-eastern Ellesmere Island and consists of predominantly Precambrian metasedimentary and crystalline rocks that extend towards Greenland. The shield is otherwise covered by the Franklinian mobile belt, which consists of sedimentary rocks that comprise the northern passive continental margin of Laurentia from Neoproterozoic to Devonian. The belt consists of infills of kilometre-thick clastic and carbonate deposits and is divided into a southeastern shelf platform and a northwestern deep-water sequence, the latter in which the Bourne Complex is located. Furthest north lies the Pearya terrane which has been interpreted as the only geologic terrane in the Canadian High Arctic that is exotic to Laurentia. The Pearya Terrane consists of Proterozoic to Silurian blocks that were placed side by side on the north margin of Laurentia during the Ellesmerian Orogeny and were severed during the Eurekan deformation which folded the clastic and carbonate sediment containing Sverdrup Basin over the Franklinian basin and developed fold-and-thrust belts as well as thrust zone and strike-slip fault zones throughout Ellesmere Island. (Trettin 1991; Trettin et al. 1998; Estrada et al. 2006; Piepjohn et al. 2016; Piepjohn and von Gosen 2018).

### ***2.2 – Bourne Complex***

The Bourne Complex comprises a hybrid assortment of greenschist-facies volcanic and sedimentary rocks and is dominated by hypabyssal mafic intrusions. The complex is exposed in the northwestern part of the Kleybolte Peninsula and the adjacent Krueger and Fjeldholmen islands. The volcanic rocks consist of tuffaceous green phyllites and andesitic flows. The sedimentary beds are poorly exposed and consist of outcrops of phyllites/slates, argillites, hornfels, and sandstones. Its thickness is undetermined as the base of the volcanic and sedimentary succession is covered and the top is eroded (Trettin 1996; Trettin et al. 1998). Three compositional igneous groups have been previously recognised (Henry 1991):

1. Subalkaline Porphyritic andesites of a subduction-related setting.
2. Transitional subduction to back-arc-related subalkaline porphyry dikes.
3. North-trending alkali dykes of a within-plate setting.

The age of the complex is unknown but estimated to be Pre-Carboniferous. The north-trending dykes cross-cut the adjacent Carboniferous Nansen Formation, and may therefore not be related to the Bourne Complex (Trettin et al. 1998). Its southwestern boundary is defined by the Kleybolte Fault Zone which separates it from serpentinitized ultramafic rocks, the Danish River formation, and upper Paleozoic strata.  $^{40}\text{Ar}$ - $^{39}\text{Ar}$  dating has previously been conducted on hornblende phenocrysts that were dated to  $380 \pm 10$  Ma (Henry 1991) and a volcanoclastic sample that was dated to  $439 \pm 2$  Ma (Powell and Schneider 2022), showing a wide discrepancy of ages. The age of the hornblende phenocrysts has been questioned as they may have undergone argon loss due to the ensuing intrusion of dykes and might not represent the actual crystallization age (Trettin 1996).

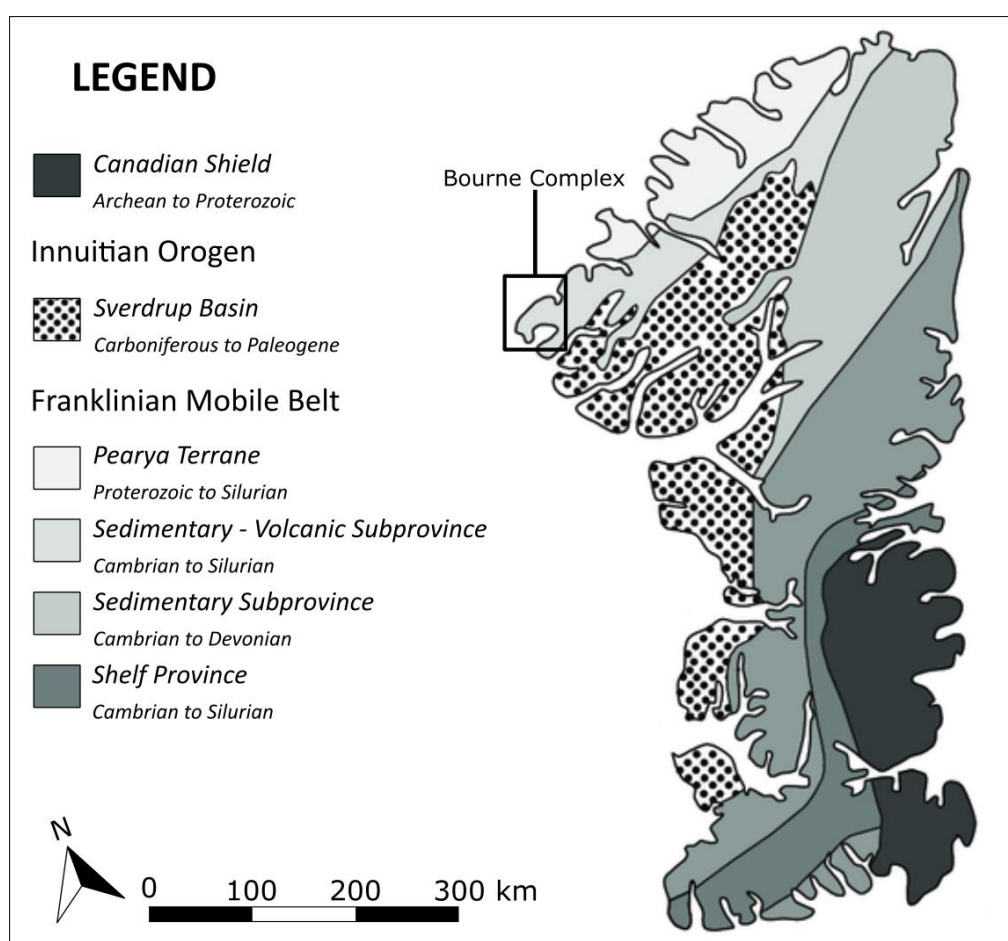


Figure 2: Simplified map showing the major tectonic units of Ellesmere Island. Note the area of study. Modified from (Trettin 1991; Atkinson 2007).

### 3 – Methods

The samples were collected by Victoria Pease during the 2017 Circum-Arctic Structural Events 19 expedition to Ellesmere Island. Seven samples were collected from the Kleybolte Peninsula and three samples from Krueger Island (Figure 3).

Twenty-two thin sections were optically assessed using a Leica DMLSP polarized light microscope. The thin sections were all scanned in plain and cross-polarised light using a Nikon Super Coolscan 9000 ED and the Nikon Scan 4.0.2 software. Major and trace element analyses of the samples were conducted using X-ray fluorescence (XRF) and laser ablation inductively coupled plasma mass spectrometry, respectively. Through petrographic and geochemical evaluation, 10 samples were selected for further analysis. The samples were selected based on the following criteria, prioritised as follows: The quality of the geochemical data, low petrographic alteration, and hand sample availability. Assessment of geochemical data consisted of evaluating the loss on ignition (LOI) levels and Fe oxidation state in each sample (Rollinson and Pease 2021). LOI was used to distinguish between fresh and altered samples as the samples were petrographically deemed to be altered and LOI is a good indicator for alteration (Haraguchi et al. 2014). Using fresh-altered LOI boundary values of 2% set by (Bas et al. 1986), a LOI level of <3% was deemed acceptable. All Fe was oxidized during sample fusion and will be referred to as Fe<sub>2</sub>O<sub>3T</sub>.

Photomicrographs of relevant thin section points were taken using the Leica Nikon Optiphot2-POL Polarizing Transmitted Light Microscope and the Leica Application Suite LAS EZ version 3.4.0 software. Point counting was subsequently performed manually using a grid containing 300 intersecting points overlain over the petrographic images and manually adjusted for each sample to cover the largest possible surface area of the thin section (See Appendix B). The mineral present at each intersecting point of the grid was counted and microscopically assessed when needed to confirm the identified mineral. The standard error of point counting was calculated using equation 1, as presented by (Plas and Tobi 1965), where X is the percentage amount of points counted for each mineral and n is the total amount of points counted.

$$2\sigma = 2 * \sqrt{\frac{X(100 - X)}{n}} \quad \text{Eq. 1}$$

The Michel-Levy Method was attempted to determine the anorthite content in plagioclase of each thin section. However, as the plagioclase crystals commonly exhibited deformation twinning, a statistically significant number of albite twins could not be located and measured. Graphs using immobile trace elements were preferred due to metamorphism and alteration (see section 4.1.3.2).

For mineral abbreviations, see Appendix A.

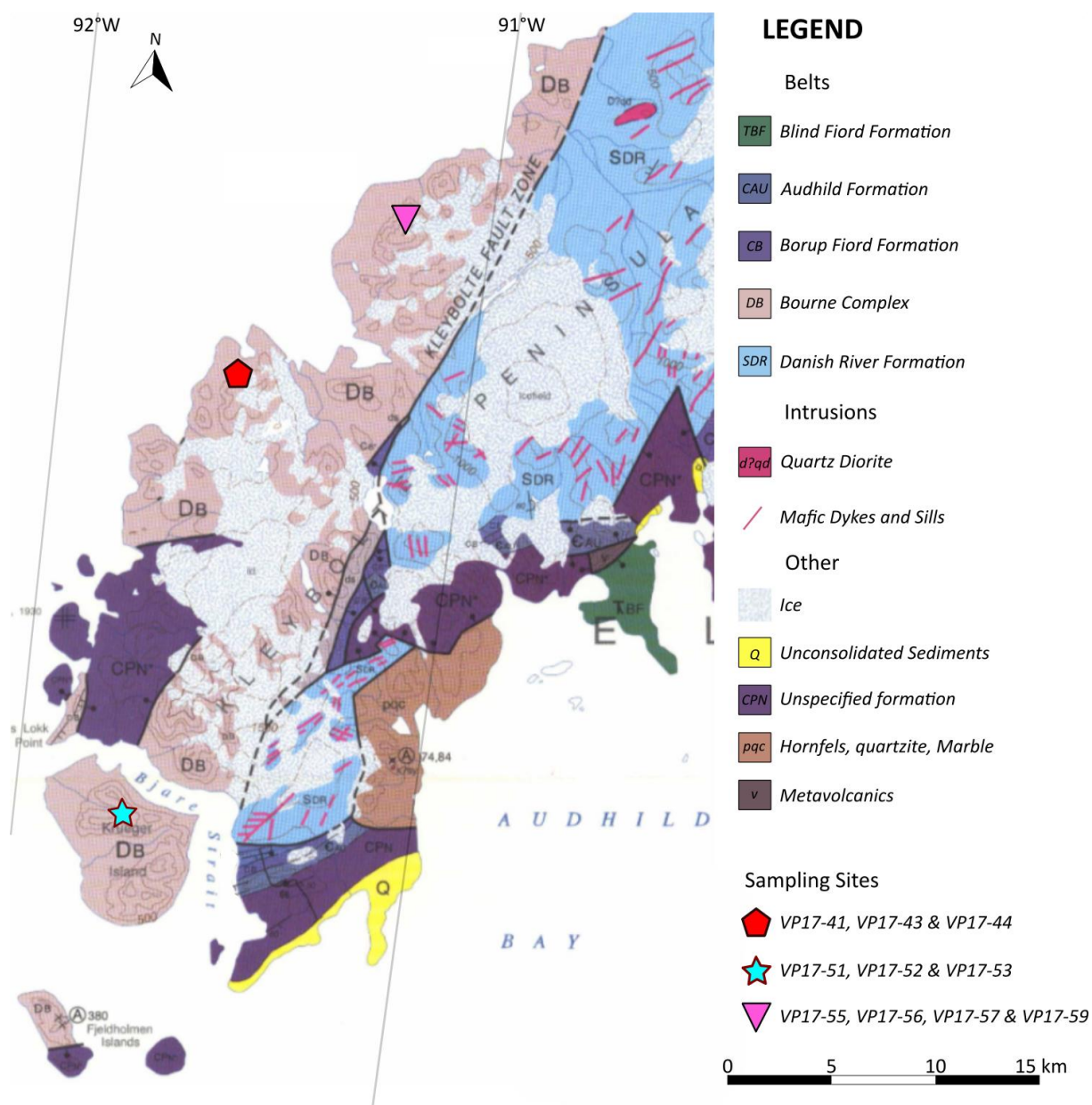


Figure 3: Map of the Bourne Complex, with sampled sections highlighted. Modified from Trettin (1996).

## 4.1 – Hand sample & Petrographic analysis

Hand sample and petrographic analysis are presented separately below. For a more detailed analysis of each sample, see Appendix D.

### 4.1.1 - Hand sample

The hand samples consist of a predominantly plagioclase groundmass, with some samples containing plagioclase phenocrysts and chlorite-altered grains. Pyroxene can be observed in varying amounts as clumped masses in all samples. Different degrees of weathering can be seen in the hand samples, varying from low to high. Some samples contain plagioclase phenocrysts varying in size from 2-7 mm on the long axis. VP17-53 differed from the rest as it contained quartz phenocrysts and lacked pyroxene.

### 4.1.2 - Petrographic Analysis

The samples divide into plutonic, volcanic, and hypabyssal types based on textural relationships. Samples VP17-41, VP17-43, VP17-44, VP17-56, VP17-57, and VP17-59 are plutonic, VP17-53 is volcanic, and VP17-51, VP17-52 and VP17-55 are hypabyssal. The Plutonic and Hypabyssal groups show very similar mineral assemblage and texture in the majority of samples, with the only major difference being that the plutonic samples commonly have porphyritic texture while the hypabyssal samples have equigranular texture. They are therefore presented together. Point counting results can be viewed below (Table 1).

Table 1: Table showing point counting results<sup>1</sup>.

Sample Type <sup>a</sup>	O q f c n " c d w p l									
	X R 3 9 6 3	X R 3 9 6 5	X R 3 9 6 6	X R 3 9 7 3	X R 3 9 7 4	X R 3 9 7 5	X R 3 9 7 7	X R 3 9 7 8	X R 3 9 7 9	X R 3 9 7 ;
Pl	59.67	58.67	50.67	56.67	53.33	47.33	56.33	50.67	56	48.67
Cpx	21.00	23.33	20.67	12.67	18	0	29	23	19.33	15
Chl	9.33	8	9.67	19.67	18	6.33	4.67	12.33	18	24
Opq	2	3.33	10	6.33	7.33	0	4.33	7.33	2.67	7
Ol	0	0	0.33	2.67	1	0	0	0	2.33	0.33
Bt	0	0	3	0.67	0	0	0	0.33	1.33	0
Kfs	0	0	0	0.33	0	10.33	0	0	0	0
Qz	0	0	0	0	0	36	0	2	0	0
Cal	0	0	0.67	1	0	0	1.67	0	0	0.33
Ep	8.00	6.67	5	0	2.33	0	4	4.33	1.67	4.67

1- See Appendix C for more details

a- P – Plutonic, V – Volcanic, H – Hypabyssal.

#### *4.1.2.1 - Plutonic and Hypabyssal*

The Plutonic and Hypabyssal samples contain a primary mineral assemblage (more than 10%) of plagioclase, clinopyroxene and chlorite and a minor amount (less than 10%) of epidote, opaque, calcite and olivine. Plagioclase is the most common mineral, accounting for 46-60% of the mineral population with habit ranging from euhedral to anhedral. Crystals are primarily tabular but sub-rounded megacrysts occur, altered and unaltered (Figure 4A). They frequently show deformation twinning and less frequently show continuous and patchy zoning. All plagioclase is altered to sericite to varying degrees from low to high (Figure 4B, 4C).

Clinopyroxene is the second most common mineral, accounting for 15-23% of the mineral population. Crystals are primarily sub-rounded, although some larger grains are tabular. Their interference colours vary significantly, up to high second order. Some crystals exhibit alteration to uraltic amphibole, generally restricted to the rims. Some tiny grains appear more like olivine than clinopyroxene and are subsequently classified as the former due to a lack of cleavage and higher interference colours. These identifications have a degree of uncertainty.

Chlorite is the primary alteration mineral, accounting for 8-24% of the mineral population. Samples show a high variance in the amount of chlorite in both plutonic and hypabyssal samples: VP17-41, VP17-43 and VP17-44 contain 8-10% chlorite and samples VP17-56, VP17-57, and VP17-59 contain 12-24% chlorite. Similarly, sample VP17-51 and VP17-52 contain 18-19.67% chlorite, while sample VP17-55 contain only 4.67% chlorite. Crystals are generally found interstitially between other minerals and show interference colours varying between green and blue. Semi-altered biotite-chlorite grains are found in some samples. The amount of clinopyroxene is directly inverse to the amount of chlorite, and the tabular shape of the chlorite crystals therefore suggests that chlorite formed after clinopyroxene (Figure 4D). Chlorite therefore seems to be the alteration product of clinopyroxene and biotite.

Epidote and calcite occur primarily as alteration minerals, with epidote primarily found as sericite and calcite predominantly as amygdale infills. Varying amounts of oxides were also present, primarily identified as hematite based on the red rims. Singular igneous amphiboles occur rarely and are altered to varying degrees (Figure 4E).

#### *4.1.2.2 - Volcanic*

Sample VP17-53 shows a volcanic texture with a primary mineral assemblage of plagioclase, quartz, and k-feldspar and a minor amount of chlorite. Plagioclase is the most common mineral, accounting for 47% of the mineral population. Its habit ranges from anhedral or euhedral and

is primarily found as fine-to-intermediate-sized crystals. Crystals frequently show deformation twinning and less frequently show patchy or oscillatory zoning. Alteration is generally low and many crystals remain unaltered. Quartz is the second most common mineral, occurring as phenocrysts and as microcrystalline groundmass. Grains are anhedral to subhedral and commonly exhibit embayed texture (figure 4F). K-feldspar is a significant accessory mineral, and its crystals commonly exhibited Carlsbad twinning. Chlorite is the primary alteration mineral but occurs in minor amounts and is generally interstitial between other crystals. A minor amount of opaques occur but the small mineral size makes them unidentifiable.

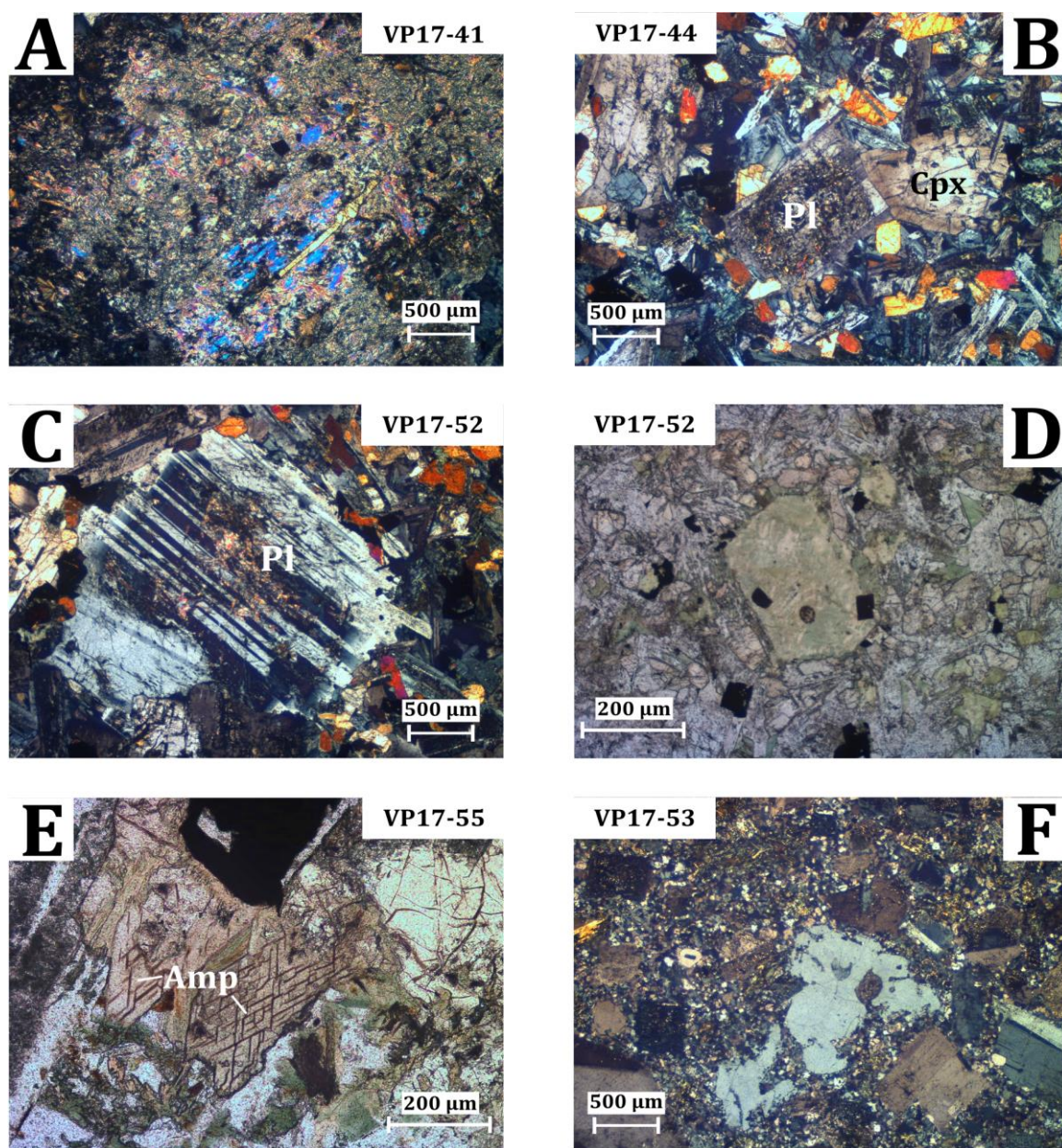


Figure 4: Microphotographs of representative igneous samples and textures: A, B) highly altered plagioclase crystals, covered in sericite. C) Slightly altered tabular plagioclase phenocryst. D) Clinopyroxene crystals that have been altered to chlorite and uralite. E) Two amphiboles. The left amphibole is visibly undergoing alteration. F). Quartz with embayed texture.

### 4.1.3 - Geochemical analysis

Major and trace elements were analyzed (Table 2).

Sample	VP17-41	VP17-43	VP17-44	VP17-51	VP17-52	VP17-53	VP17-55	VP17-56	VP17-57	VP17-59
<i>wt(%)</i>										
SiO <sub>2</sub>	48.1	49.2	48.9	49.62	48.98	68.60	50.15	49.45	50.76	50.2
Al <sub>2</sub> O <sub>3</sub>	17.7	17.1	14.0	15.07	18.47	15.63	15.36	14.50	18.36	15.4
CaO	10.6	10.7	8.80	9.23	11.36	2.43	10.34	9.21	9.87	8.63
MgO	5.86	6.19	4.72	5.23	5.41	1.26	5.28	4.67	5.52	4.31
MnO	0.19	0.19	0.26	0.24	0.18	0.05	0.20	0.24	0.17	0.24
P <sub>2</sub> O <sub>5</sub>	0.23	0.17	0.27	0.22	0.13	0.11	0.25	0.38	0.16	0.27
Fe <sub>2</sub> O <sub>3</sub>	11.1	10.7	15.8	13.8	10.3	5.41	12.7	14.6	9.24	14.0
Na <sub>2</sub> O	3.0	3.1	3.6	3.62	2.86	4.97	3.19	3.70	3.53	4.3
K <sub>2</sub> O	1.3	1.0	0.78	0.90	0.84	1.1	0.60	0.41	1.1	0.75
TiO <sub>2</sub>	2.03	1.70	2.80	2.10	1.45	0.45	1.95	2.81	1.32	1.92
Total	100.0	100.0	100.0	100.0	100.0	100.0	100.0	100.0	100.0	100.0
LOI	2.7	2.3	1.5	2.0	1.8	1.4	2.5	2.1	2.4	2.8
<i>ppm</i>										
Ba	99.9	154.4	133.8	225.5163	141.5	179.7	98.7	100.3	175.5	135.0
Cr	147.0	185.2	37.45	56.09285	111.6	133.3	56.1	52.3	153.0	40.0
Cs	0.26	0.19	0.70	0.07977	0.14	0.43	0.12	bd	0.22	0.36
Cu	51.84	43.65	52.34	73.46217	65.94	45.71	31.36	38.12	52.29	28.34
Ga	17.00	16.04	18.77	17.50705	14.63	14.87	16.70	20.13	16.65	23.21
Hf	3.82	3.18	4.65	3.601655	2.27	3.90	3.49	5.46	4.59	4.48
Nb	10.6	4.04	9.81	19.37225	12.93	7.89	7.86	14.05	10.01	7.78
Ni	61.7	32.7	17.5	26.88215	38.5	5.6	22.7	20.8	43.9	20.9
Pb	2.6	2.4	2.7	7.658304	3.2	6.4	2.4	3.0	1.7	6.8
Rb	32.9	23.9	13.2	17.2818	17.6	22.8	10.1	4.5	20.2	11.3
Sc	32.4	40.8	41.4	39.42003	35.1	11.1	32.9	35.3	30.5	36.4
Sr	345.0	314.6	257.9	243.7255	330.3	239.4	320.7	228.1	275.5	146.7
Ta	0.62	0.26	0.60	0.96212	0.68	0.57	0.47	0.86	0.66	0.49
Th	1.58	1.45	1.55	1.40609	0.94	6.13	2.46	2.71	3.23	4.57
U	0.47	0.50	0.44	0.306731	0.2	2.5	0.6	0.8	0.9	1.4
V	240	231	393	303.2442	215	46	257	301	176	414
Y	32.2	31.2	44.2	39.9288	24.8	16.8	33.8	46.6	31.3	40.5
Zr	161	131	195	157.2181	97	177	152	221	186	156
La	11.3	7.90	12.9	12.51493	8.4	18.5	14.1	17.8	13.1	21.7
Ce	25.6	19.4	30.0	27.16413	17.7	34.1	30.6	39.0	30.2	45.0
Pr	3.93	3.06	4.55	3.928919	2.58	3.84	4.43	6.02	4.26	6.61
Nd	18.6	15.9	22.0	17.86586	11.6	14.3	19.7	28.0	17.9	27.6
Sm	5.31	4.63	6.39	5.381539	3.34	3.19	5.59	7.71	5.02	8.66
Eu	1.83	1.71	2.27	1.905037	1.32	1.23	1.78	2.70	1.52	2.63
Gd	5.43	4.94	6.99	6.057229	3.78	3.09	5.65	8.81	5.58	7.88
Tb	0.908	0.848	1.24	1.026676	0.616	0.491	0.948	1.431	0.906	1.418
Dy	6.04	5.71	7.92	6.941199	4.26	2.97	6.13	8.95	6.13	8.93
Ho	1.21	1.23	1.72	1.491647	0.95	0.59	1.27	1.90	1.25	1.75
Er	3.57	3.48	4.83	4.305157	2.76	1.63	3.63	5.21	3.74	4.99
Tm	0.513	0.500	0.686	0.59416	0.387	0.222	0.501	0.731	0.524	0.691
Yb	3.47	3.34	4.73	4.471587	2.741573	1.68	3.55	5.24	3.79	4.83
Lu	0.483	0.461	0.647	0.605808	0.38053	0.294	0.512	0.745	0.521	0.662

Table 2: Table showing geochemical analyses of the 10 samples from the Bourne Complex.

Rare earth elements (REE) and multielement diagrams (Figure 5) show trends normalized to primitive mantle (PM) values from (Sun and McDonough 1989). These diagrams reveal that the samples have trace element patterns similar to enriched mid-ocean ridge basalt (E-MORB) with highly enriched LREE concentrations that approach Ocean-island-basalt (OIB) like signatures.

#### 4.1.3.1.1 –Plutonic samples

Volatile content from LOI ranges from 1.5-2.8 wt%. SiO<sub>2</sub> content for the plutonic samples ranges from 48.1-50.8 wt%, Al<sub>2</sub>O<sub>3</sub> ranges from 14.0-18.4 wt%, Fe<sub>2</sub>O<sub>3T</sub> from 9.2-15.8 wt%, CaO from 8.6-10.7 wt%, MgO from 4.3-6.2 wt%, MnO from 0.2-0.3 wt%, P<sub>2</sub>O<sub>5</sub> from 0.2-0.4%, Na<sub>2</sub>O from 3.0-4.3 wt%, K<sub>2</sub>O from 0.4-1.3 wt%., and TiO<sub>2</sub> from 1.3-2.8 wt%.

Trace element measurements reveal low to moderate LREE enrichment relative to HREE ( $L_{aPM}/L_{uPM} = 1.84 - 3.53$ ) and a flat HREE trend ( $Tb_{PM}/Yb_{PM} = 1.09 - 1.34$ ). Eu anomalies are flat to very weak ( $Eu_{PM}/Eu^* = 0.88 - 1.09$ ). Sample VP17-43 shows a pronounced Ta-Nb anomaly and sample VP17-56 shows a pronounced Rb anomaly. Samples VP17-56, VP17-57 and VP17-59 have positive Th anomalies, while VP17-41, VP17-42 and VP17-44 have flat Th trends.

#### 4.1.3.1.1 –Volcanic sample

The sample has a LOI content of 1.4 wt%. The volcanic samples has the following elemental content: 68.6 wt% SiO<sub>2</sub>, 15.6 wt% Al<sub>2</sub>O<sub>3</sub>, 5.41 wt% Fe<sub>2</sub>O<sub>3T</sub>, 2.43 wt% CaO, 1.26 wt% MgO, 0.05 wt% MnO, 0.11 wt% P<sub>2</sub>O<sub>5</sub>, 4.97 wt% Na<sub>2</sub>O, 1.1 wt% K<sub>2</sub>O and 0.45 wt% TiO<sub>2</sub>.

The sample shows high LREE enrichment relative to HREE ( $L_{aPM}/L_{uPM} = 6.74$ ) and a flat HREE trend ( $Tb_{PM}/Yb_{PM} = 1.34$ ) but is more depleted in HREE compared to other samples. Furthermore, it shows a slightly positive Eu anomaly ( $Eu_{PM}/Eu^* = 1.2$ ), very positive Th anomaly, and negative Ti and P anomalies.

#### 4.1.3.1.1 –Hypabyssal samples

Volatile content from LOI ranges from 1.5-2.5 wt%. SiO<sub>2</sub> content for the hypabyssal samples ranges from 48.9-50.1 wt%, Al<sub>2</sub>O<sub>3</sub> from 14.0-18.5 wt%, Fe<sub>2</sub>O<sub>3T</sub> from 12.7-13.8 wt%, CaO from 8.8-11.4 wt%, MgO from 4.7-5.4 wt%, MnO and P<sub>2</sub>O<sub>5</sub> values are at 0.2 wt% in all hypabyssal samples, Na<sub>2</sub>O from 3.2-3.6 wt%, K<sub>2</sub>O from 0.6-0.9 wt%., and TiO<sub>2</sub> from 2.0-2.1 wt%.

Trace element measurements show low LREE enrichment relative to HREE ( $L_{aPM}/L_{uPM} = 2.23 - 2.97$ ) and a flat HREE trend ( $Tb_{PM}/Yb_{PM} = 1.03 - 1.22$ ). Sample VP17-52 has a weak positive Eu anomaly while the other two lack an Eu anomaly ( $Eu_{PM}/Eu^* = 0.97 - 1.14$ ) and it's more

depleted in HREE relative to the other hypabyssal samples. Sample VP17-51 and VP17-52 also have positive Ta-Nb anomalies, while VP17-55 has a weak Ta-Nb anomaly.

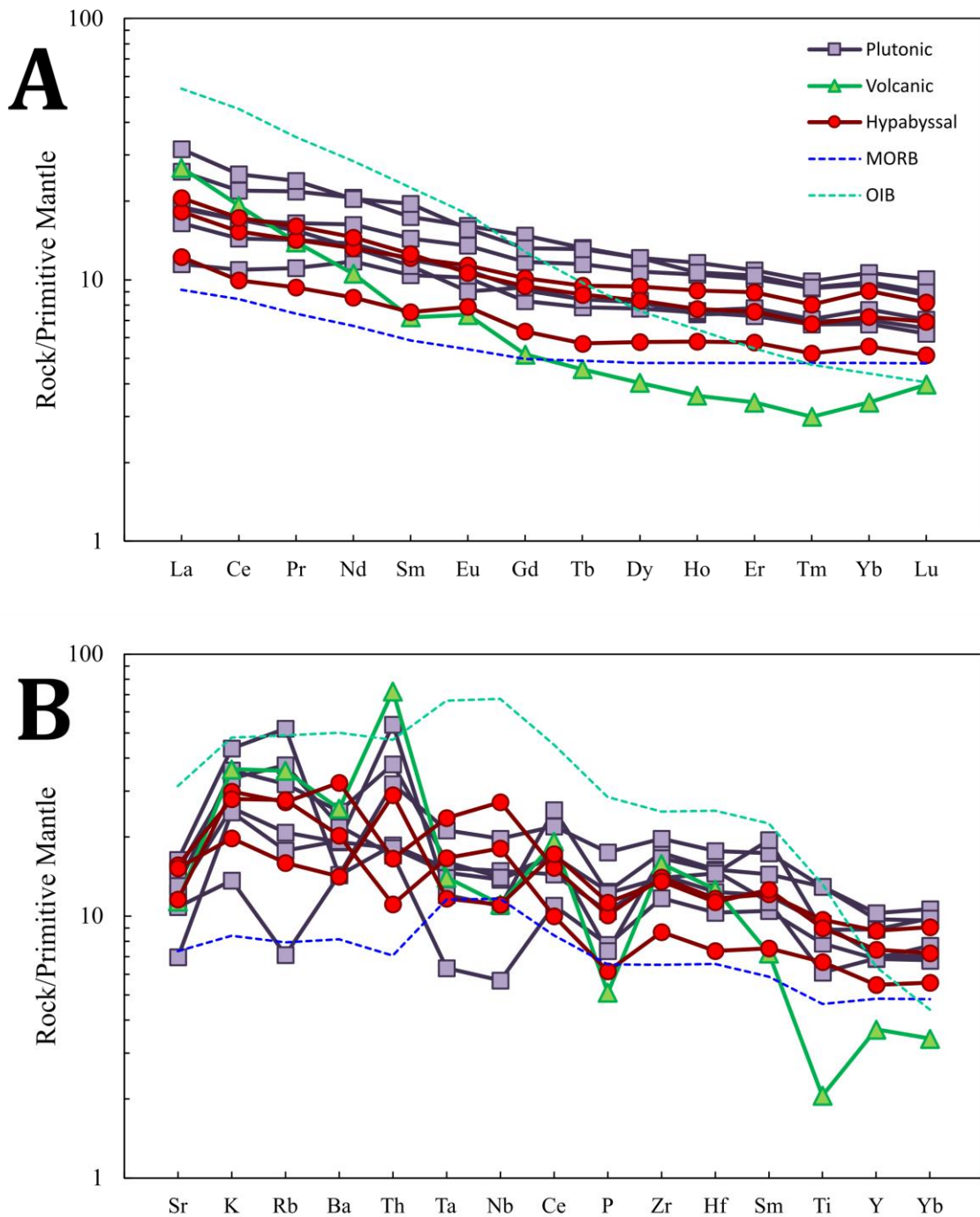


Figure 5: Trace element diagrams, normalized to primitive mantle (Values from Sun & McDonough, 1989) A) REE diagram. B) Multielement diagram.

## **5 - Discussion**

Petrographical analysis may be sufficient to classify fresh rocks but altered and/or metamorphosed samples with potentially altered minerals require geochemical analyses. Geochemical analyses also need to be evaluated for element mobility, and the two methods should be carefully combined. Geochemical data is also needed to identify signatures associated with specific tectonic settings.

### ***5.1 - Selection of diagrams, metamorphic alteration and element mobility***

Discrimination diagrams used to classify rocks commonly utilize major elements. For example, the International Union of Geological Sciences (IUGS) recommend the TAS discrimination diagram by (Bas et al. 1986) for volcanic rocks (Pearce 1996), and the discrimination diagram made by (Wilson 1989) that utilizes discrimination fields by (Cox et al. 1979) for plutonic rocks (Lustrino et al. 2022). Both diagrams use K and Na to classify rocks, which are mobile during metamorphism and alteration and therefore cannot be reliably used to classify rocks that have been metamorphosed or largely geochemically altered. Certain elements generally retain immobility during secondary alteration processes and can thus be used to assess altered or metamorphosed samples. These are referred to as immobile elements and consist of Ti, Zr, Hf, Nb, Ta, Cr, Th, Al, Ga and all rare earth elements (REE) except for La (Winchester and Floyd 1977; Pearce 1996; Hastie et al. 2007). However, some immobile elements have been known to mobilise in specific circumstances: Th for example may mobilize during alteration and weathering (Bienvenu et al. 1990). It is therefore important to screen for immobile element mobilization in altered, weathered or metamorphosed samples.

Petrographical analysis of the samples shows pervasive greenschist-facies metamorphic conditions and various degrees of alteration and weathering, as well as LOI levels above 2% on seven samples. These conditions indicate possible major and trace element mobilisation (MacLean 1990) and the immobile elements should therefore be assessed on whether they retain immobility during alteration and metamorphism. To assess this, the  $Al_2O_3/Na_2O$  alteration index of (Spitz and Darling 1978) was used, which uses an immobile and mobile element to determine if immobile samples may have become mobile, with a set threshold of 10. All samples showed index ratios below the set threshold (Appendix E) and were deemed suitable for analytical use.

## 5.2 – Cogenetic magma series

Pearce element ratio diagrams and Harker diagrams were combined to determine if the samples share a cogenetic magma series (Figure 6, 7). A trend is not visible on the Harker diagrams due to the limited sample size which severely limits Harker diagrams, but it is evident from the bivariate plots that the volcanic and hypabyssal samples exhibit similar compositional characteristics and may thus be cogenetic magmas related by crystal fractionation of plagioclase. Conversely, the volcanic sample diverges significantly from this trend and therefore appears to represent a distinct magma series. Furthermore, as SiO<sub>2</sub> increases with magmatic evolution (Winter 2014), sample VP17-41 appears to be the parent magma as it has the lowest silica content.

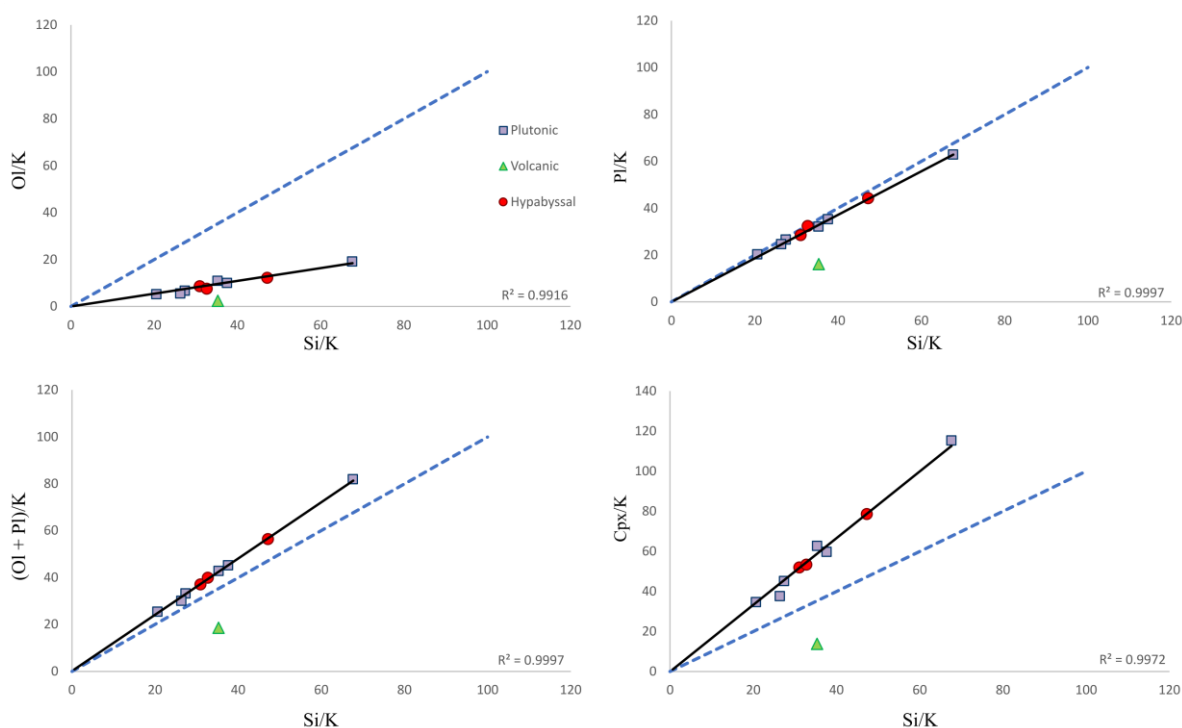


Figure 6: Pearce element ratios. The plutonic and hypabyssal samples seem to be related through Pl and Ol + Px fractionation.

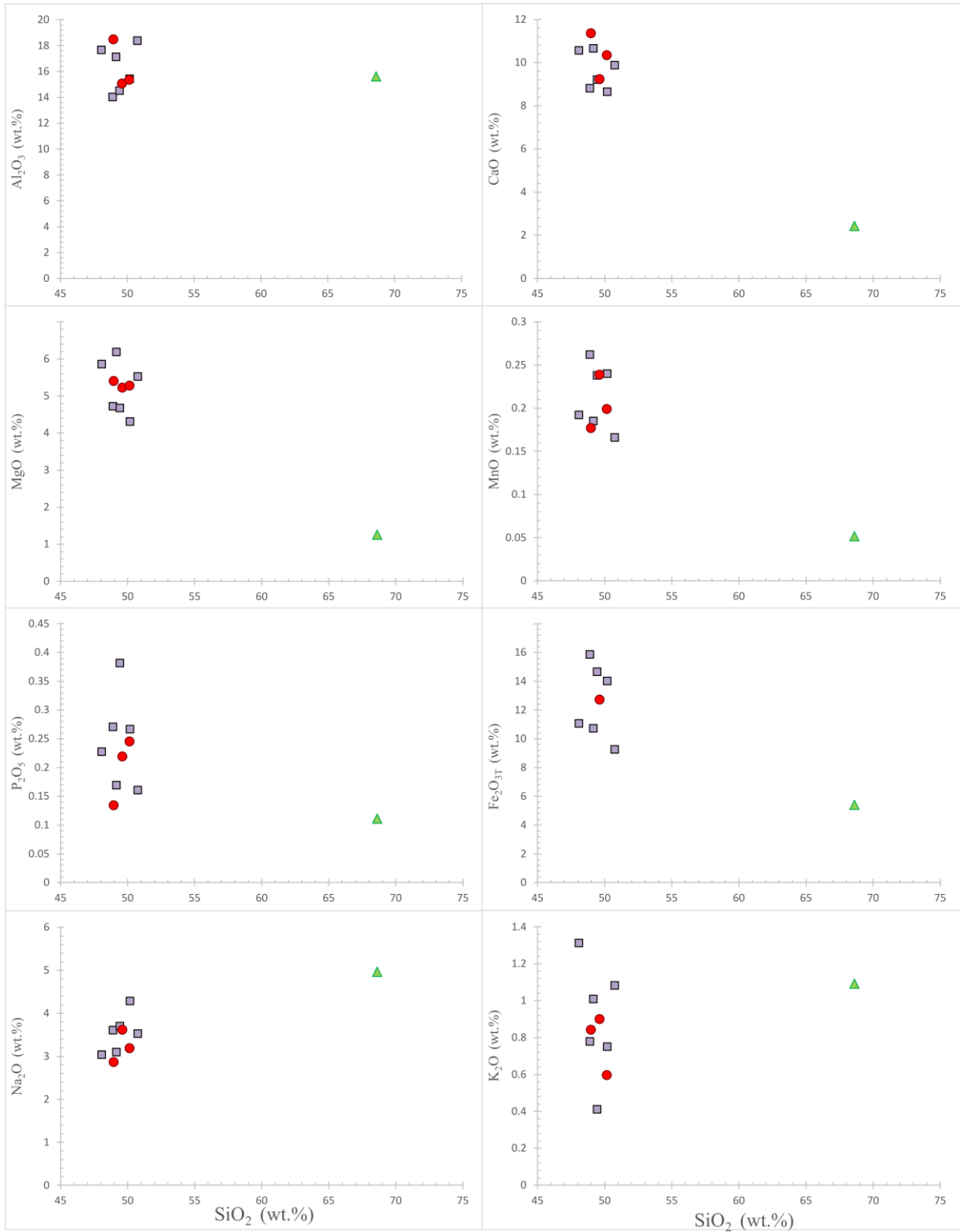


Figure 7: Harker diagrams. The plutonic and hypabyssal samples group up without the volcanic sample.

### 5.3 – Sample classification & metamorphic facies

IUGS modal classification diagrams (Appendix F) classify the plutonic samples as leucogabbros, volcanic sample as a dacite and hypabyssal samples as gabbro/basalts, thereby deemed to be dolerites. Geochemical diagrams classify all samples as subalkaline and as basalts except for two samples (VP17-53 and VP17-57) that plot as andesite or basaltic andesite transitional to basalt and dacite respectively (Figure 8). The samples belong to a calc-alkaline to transitional magma series (Figure 9), differing from Henry's predominantly calc-alkaline samples. The presence of plagioclase, clinopyroxene, and alteration products indicates greenschist facies metamorphism, which would reflect metamorphic conditions of 300–500°C and 2–8 Kbar (Klein and Philpotts 2013).

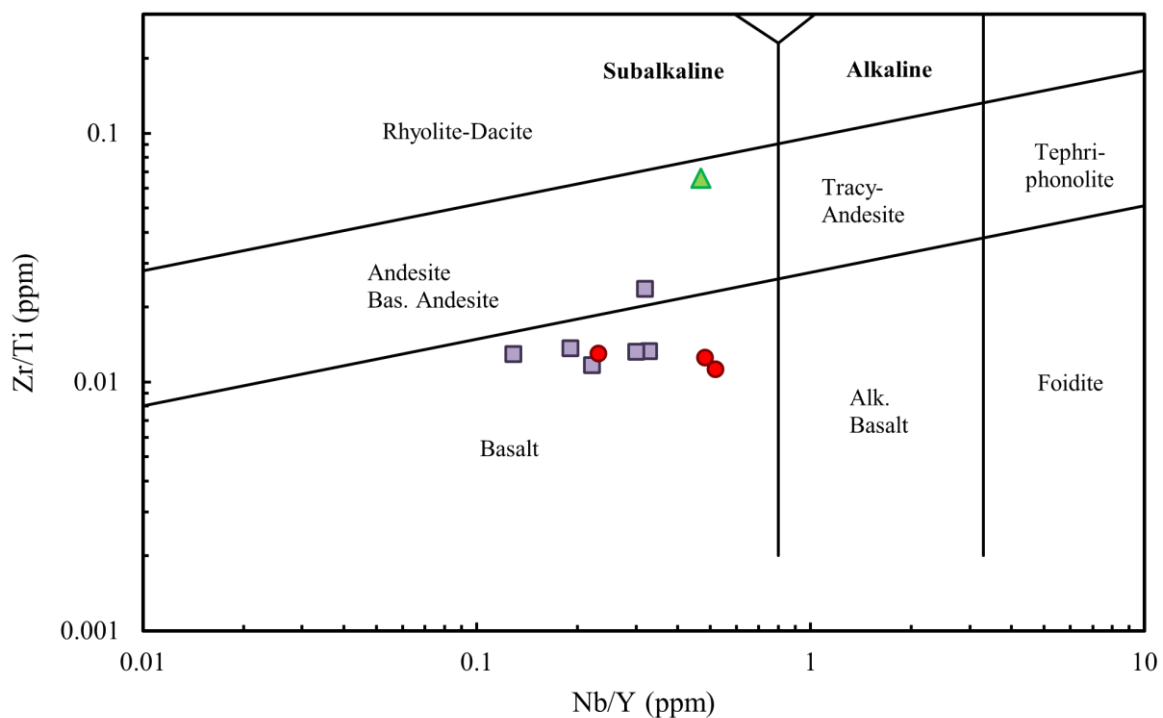


Figure 8: Zr/Ti vs. Nb/Y classification diagram (Pearce 1996). The samples are generally subalkaline and basaltic in composition but two plot as transitional andesites.

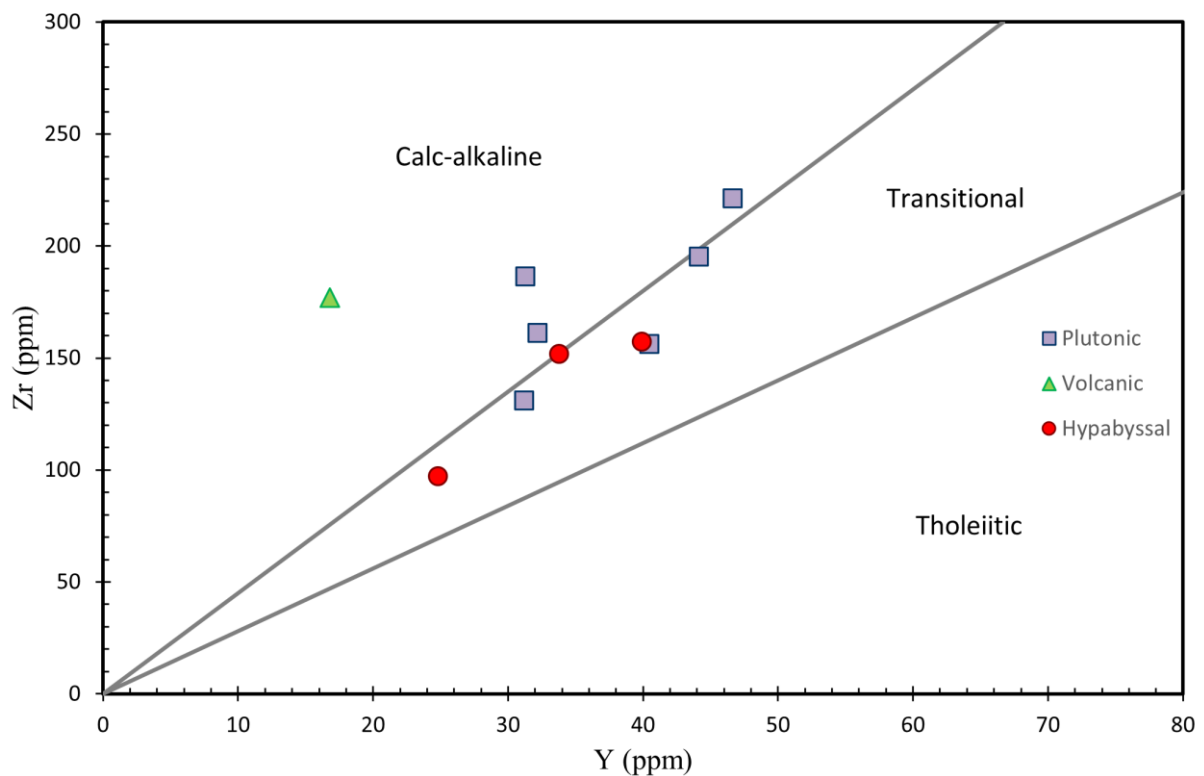


Figure 9: Zr/Y magmatic affinity diagram (Ross and Bédard 2009). The samples all plot as calc-alkaline to transitional.

#### 5.4 – Tectonic setting

REE and multielement diagram trends can be used to infer possible mantle source region(s) and depth depending on chemical signature and the minerals present. Plagioclase, spinel, and garnet are stable at shallow, intermediate, and deep depths respectively and show unique chemical signatures. Plagioclase-bearing shallow mantle sources are characterized by low to moderate LREE enrichment and a flat HREE trend, as well as the presence of Eu and Sr anomalies. Spinel-bearing intermediate mantle sources show identical REE trends but lack Eu and Sr anomalies. Spinel grains should also be found in petrographic analysis. Garnet-bearing deep mantle sources show high LREE enrichment relative to HREE and a strong negative HREE trend. The samples show LREE enrichment relative to HREE and a flat HREE trend, arguing against a garnet-bearing source and subsequently against a deep mantle source (Winter 2014). Similarly, the absence of Eu anomalies goes against a plagioclase-bearing shallow mantle source, leaving spinel as the only possible source.

Calc-alkaline rocks are widespread in arc-related settings and thus typically viewed as related to subduction zones. However, regions undergoing extension and rifting have erupted calc-

alkaline magma in several regions, and care should therefore be taken in viewing the occurrence of calc-alkaline rocks as proof of a subduction-related setting. The Th/Nb classification diagram shows that half the samples are classified as originating from a convergent setting and half from a divergent setting (Figure 10). Ti/V log-log plots also give MORB-OIB transitional classifications similar to the REE and multielement diagrams (Figure 11). The samples have contradictory characteristics indicative of different magmatic environments. The REE and multielement diagrams define characteristics between OIB and E-MORB and show LREE enrichment and a flat HREE trend, which argues against a deep, garnet-bearing mantle source typically associated with OIB. They also show varying Nb and Ta anomalies that range from weakly negative to positive. All arc-related basaltic lavas have negative Nb and Ta anomalies (Xia and Li 2019), suggesting that these samples originate elsewhere.

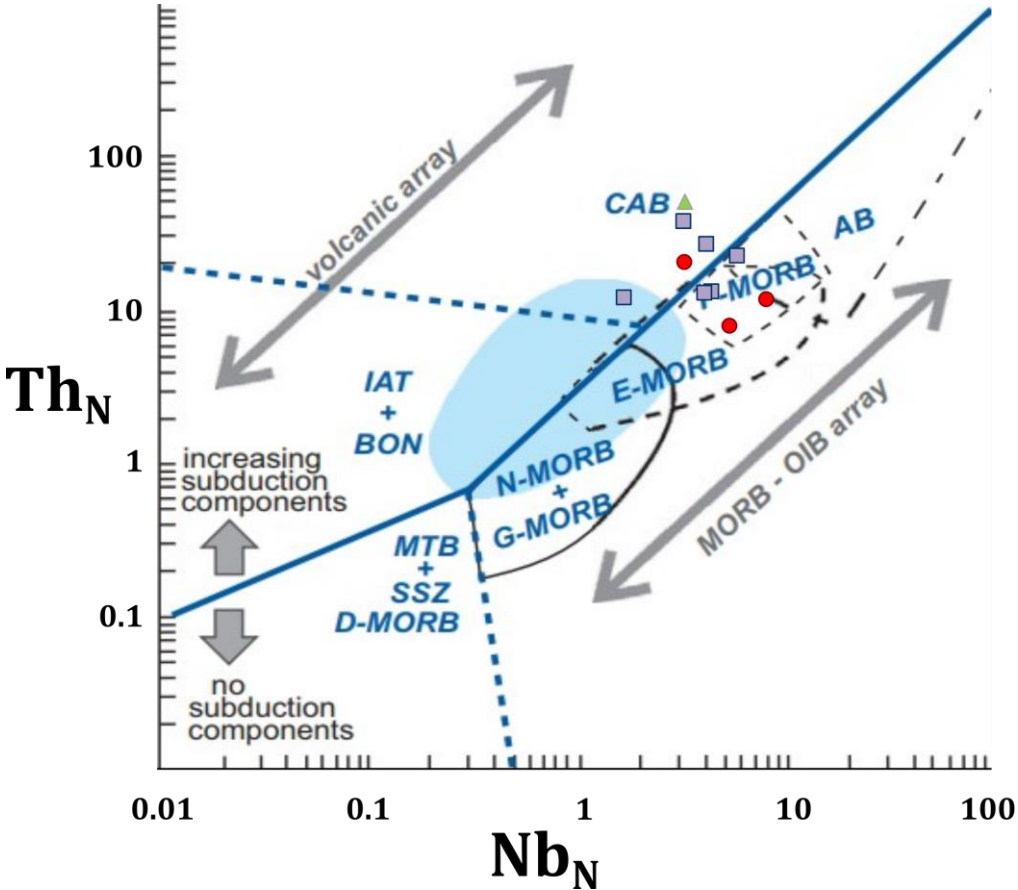


Figure 10: Classification of ophiolite-related basalts by (Saccani 2015). Values normalized to N-Morb from Sun & McDonough (1989). Image taken from (Rollinson and Pease 2021). AB – Alkaline basalt, MORB – mid-ocean ridge basalt, N-MORB – normal MORB, E-MORB – enriched MORB, P-MORB – Plume MORB, G-MORB – garnet MORB, D-MORB – depleted MORB, CAB – Continental arc basalt, IAT – Island arc tholeiite, BON = Boninite, MTB – medium-Ti basalt, SSZ – Supra subduction zone.

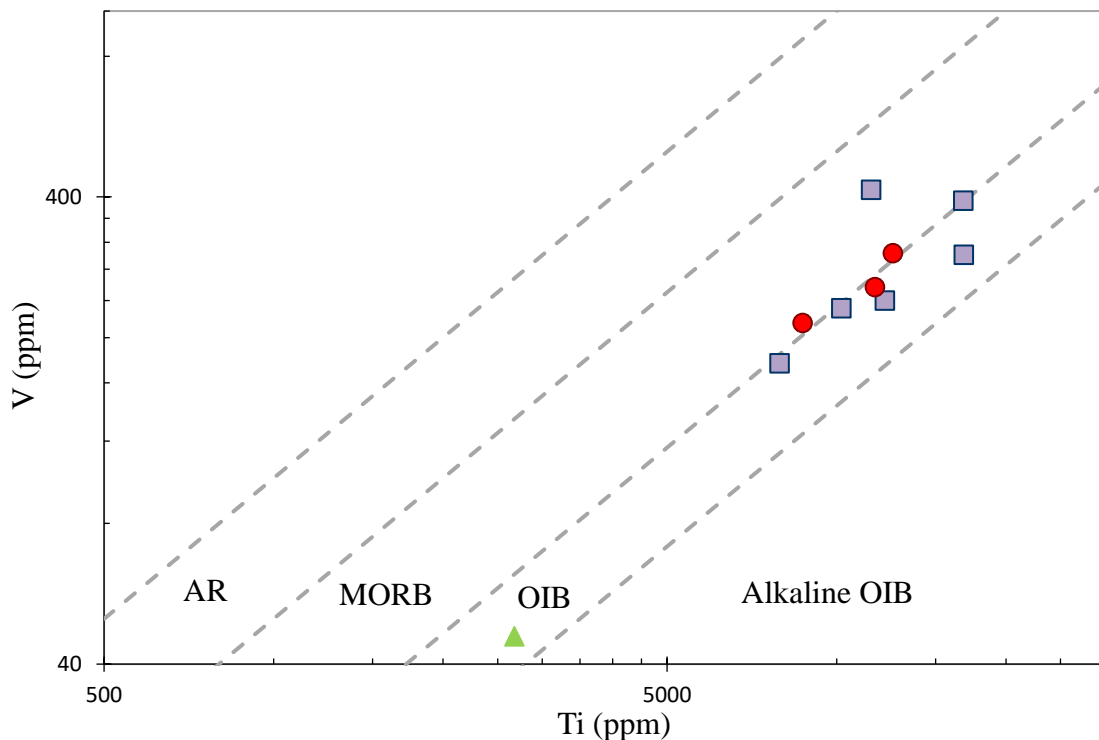


Figure 11: Ti/V log-log plot from showing transitional MORB-OIB classification (Shervais 2022).

The occurrence of transitional geochemistry with enriched trace elements and subduction-related characteristics is instead more consistent with a continental intraplate setting that may become contaminated through interaction with continental crust, which is corroborated by the samples within-plate signature (Figure 12).

Continental intraplate basalts are generated in extensional environments within continental plates, generally due to adiabatic upwelling of the convecting mantle (Chen et al. 2022), and are generally associated with large igneous provinces. Contamination from continental crust can bestow subduction-like signatures in continental intraplate basalts. Uncontaminated intracontinental basalts are typically alkaline and lack Nb and Ta anomalies, while contaminated intracontinental basalts classify as both subalkaline and alkaline and have subduction-like negative Ta and Nb anomalies as well as elevated Th content. They also show Ti/V ratios that overlap MORB and OIB fields in the Ti/V diagram, similar to samples from the Bourne Complex (Xia and Li 2019; Shervais 2022). The E-MORB signature and intermediate mantle depth could indicate that the samples originated from the melting of a MORB-like mantle source, which would impart some MORB-like geochemical signatures (e.g. Shafeie et

al. (2016). A recent study by Faehnrich et. al (2023) proposed that the near-lying Yelverton formation origin originated from a rifting event along the Laurentian margin circa 570-530 Ma, and although current age dating indicates a difference of 100 Ma between the two locations, this does not necessarily imply a lack of relation between them. Further isotopic analysis and geochronological dating of samples from the Bourne complex would be required to ascertain this with greater certainty.

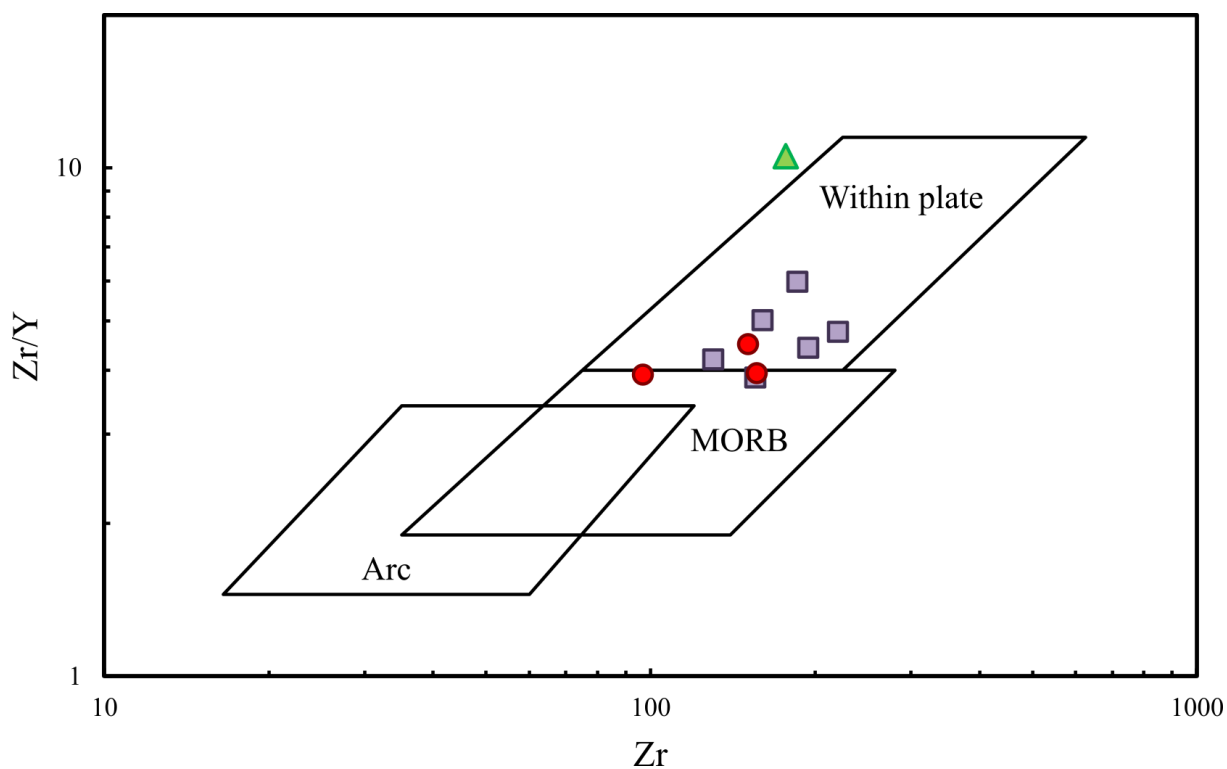


Figure 12: Zr/Zr/Y diagram, showing within-plate-like characteristics (Pearce and Norry 1979).

## Conclusion

- The samples were petrographically classified as six leucogabbros, one dacite, and three dolerites, and geochemically classified as subalkaline transitional to calc-alkaline basalts and andesites. The samples have undergone greenschist-facies metamorphism.
- Bivariate plots suggest that the plutonic and hypabyssal samples could be related through a cogenetic magma series, while the volcanic one belongs to a separate series.
- PER diagrams are consistent with shallow crystal fractionation of plagioclase.
- REE trends and mineral occurrence suggest that samples originate from a spinel-bearing mantle source.
- Samples show trace element ratios characteristic of convergent and divergent trace elements but lack subduction-related signatures. They instead closely resemble those of contaminated continental intraplate settings. This may be related to rifting along the Laurentian margin, but further studies are required to confirm.

## **Acknowledgements**

I would like to sincerely thank my supervisor Victoria Pease for providing me with this thesis and patiently teaching and helping me these last two months. I would also like to thank my family and friends for supporting me throughout this endeavour.

## References

- Atkinson N. 2007. A statistical technique for determining the source area of glacially transported granite erratics in the Queen Elizabeth Islands, Nunavut. *Canadian Journal of Earth Sciences*. 44:43–59. <https://doi.org/10.1139/E06-067>
- Bas MJL, Maitre RWL, Streckeisen A, Zanettin B, IUGS Subcommission on the Systematics of Igneous Rocks. 1986. A Chemical Classification of Volcanic Rocks Based on the Total Alkali-Silica Diagram. *Journal of Petrology*. 27(3):745–750. <https://doi.org/10.1093/petrology/27.3.745>
- Bienvenu P, Bougault H, Joron JL, Treuil M, Dmitriev L. 1990. MORB alteration: Rare-earth element/non-rare-earth hygromagmaphile element fractionation. *Chemical Geology*. 82:1–14. [https://doi.org/10.1016/0009-2541\(90\)90070-N](https://doi.org/10.1016/0009-2541(90)90070-N)
- Chen Q, Liu H, Johnson T, Hartnady M, Kirkland CL, Lu Y, Sun W. 2022. Intraplate continental basalts over the past billion years track cooling of the mantle and the onset of modern plate tectonics. *Earth and Planetary Science Letters*. 597:117804. <https://doi.org/10.1016/j.epsl.2022.117804>
- Cox KG, Bell JD, Pankhurst RJ. 1979. Quaternary systems. In: Cox KG, Bell JD, Pankhurst RJ, editors. *The Interpretation of Igneous Rocks* [Internet]. Dordrecht, Netherlands: Springer Netherlands; p. 197–221. [https://doi.org/10.1007/978-94-017-3373-1\\_8](https://doi.org/10.1007/978-94-017-3373-1_8)
- Esri. 2024. World Imagery [Internet]. [accessed 2024 Jun 8]. <https://www.arcgis.com/home/item.html?id=10df2279f9684e4a9f6a7f08febac2a9>
- Estrada S, Piepjohn K, Henjes-Kunst F, Gosen W. 2006. Geology, Magmatism and Structural Evolution of the Yelverton Bay Area, Northern Ellesmere Island, Arctic Canada. *Polarforschung*. 73:59–75.
- Faehnrich K, McClelland WC, Webb L, Kościńska K, Strauss JV. 2023. Late Ediacaran–early Cambrian rifting along the northern margin of Laurentia: constraints from the Yelverton Formation of Ellesmere Island, Canada. *Can J Earth Sci*. 60(12):1597–1626. <https://doi.org/10.1139/cjes-2023-0020>
- Haraguchi S, Ishizuka H, Ishii T, Fujioka K, Yuasa M, Shibasaki H. 2014. Low- and high-temperature alterations of volcanic rocks in the northwestern Philippine Sea, and association with volcanic settings. *Island Arc*. 23:324–343. <https://doi.org/10.1111/iar.12078>
- Hastie AR, Kerr AC, Pearce JA, Mitchell SF. 2007. Classification of Altered Volcanic Island Arc Rocks using Immobile Trace Elements: Development of the Th–Co Discrimination Diagram. *Journal of Petrology*. 48(12):2341–2357. <https://doi.org/10.1093/petrology/egm062>
- Henry AS. 1991. *The Petrochemistry and Origin of the Bourne Complex, Northwestern Ellesmere Island, Canada* [Bachelor's Thesis]. Halifax, Nova Scotia: Dalhousie University.
- Klein C, Philpotts AR. 2013. *Earth Materials: Introduction to Mineralogy and Petrology*. New York: Cambridge University Press.

Koch MM, Faehnrich K, McClelland WC, Crowley JL, Melchin MJ, Beranek LP, Strauss JV. 2022. Age and significance of the Fire Bay assemblage: an Ordovician arc fragment within the Clements Markham belt, northwestern Ellesmere Island, Canada. *Can J Earth Sci.* 59(10):639–659. <https://doi.org/10.1139/cjes-2021-0129>

Lustrino M, Bonin B, Day J, Doroshkevich A, Guo Z, Kerr A, Heilborn M, Ivanov A, Mitchell R, Nakagawa M, et al. 2022. IUGS Task Group on Igneous Rocks. Beijing, China: International Union of Geological Sciences.

MacLean WH. 1990. Mass change calculations in altered rock series. *Mineralium Deposita.* 25(1):44–49. <https://doi.org/10.1007/BF03326382>

Pearce JA. 1996. A user's guide to basalt discrimination diagrams. Trace element geochemistry of volcanic rocks: applications for massive sulphide exploration Geological Association of Canada, Short Course Notes. 12:79–113.

Pearce JA, Norry MJ. 1979. Petrogenetic implications of Ti, Zr, Y, and Nb variations in volcanic rocks. *Contributions to Mineralogy and Petrology.* 69(1):33–47. <https://doi.org/10.1007/BF00375192>

Piepjohn K, von Gosen W. 2018. Structural transect through Ellesmere Island (Canadian Arctic): superimposed Palaeozoic Ellesmerian and Cenozoic Eureka deformation. *Geological Society, London, Special Publications.* 460(1):33–56. <https://doi.org/10.1144/SP460.5>

Piepjohn K, von Gosen W, Tessensohn F. 2016. The Eureka deformation in the Arctic: an outline. *Journal of the Geological Society.* 173(6):1007–1024. <https://doi.org/10.1144/jgs2016-081>

Plas L v. d., Tobi AC. 1965. A chart for judging the reliability of point counting results. *American Journal of Science.* 263:87–90. <https://doi.org/10.2475/ajs.263.1.87>

Powell JW, Schneider DA. 2022. Phanerozoic Record of Northern Ellesmere Island, Canadian High Arctic, Resolved Through  $^{40}\text{Ar}/^{39}\text{Ar}$  and (U-Th)/He Geochronology. *Tectonics.* 41(9):e2021TC007065. <https://doi.org/10.1029/2021TC007065>

Rollinson H, Pease V. 2021. *Using Geochemical Data: To Understand Geological Processes [Internet].* 2nd ed. Cambridge: Cambridge University Press. <https://doi.org/10.1017/9781108777834>

Ross P-S, Bédard JH. 2009. Magmatic affinity of modern and ancient subalkaline volcanic rocks determined from trace-element discriminant diagrams. *Can J Earth Sci.* 46(11):823–839. <https://doi.org/10.1139/E09-054>

Saccani E. 2015. A new method of discriminating different types of post-Archean ophiolitic basalts and their tectonic significance using Th-Nb and Ce-Dy-Yb systematics. *Geoscience Frontiers.* 6(4):481–501. <https://doi.org/10.1016/j.gsf.2014.03.006>

Shafeie Z, Ali Arian M, Haghaziar S, Abedini MV. 2016. Geochemistry and Petrogenesis of Tertiary Volcanic Rocks of the Eastern Roodbar, Alborz Mountain, North of Iran. *OJG.* 06(10):1296–1311. <https://doi.org/10.4236/ojg.2016.610095>

Shervais JW. 2022. The petrogenesis of modern and ophiolitic lavas reconsidered: Ti-V and Nb-Th. *Geoscience Frontiers*. 13(2):101319. <https://doi.org/10.1016/j.gsf.2021.101319>

Spitz G, Darling R. 1978. Major and minor element lithochemical anomalies surrounding the Louvem copper deposit, Val d'Or, Quebec. *Can J Earth Sci*. 15(7):1161–1169. <https://doi.org/10.1139/e78-122>

Streckeisen A. 1976. To each plutonic rock its proper name. *Earth-Science Reviews*. 12(1):1–33. [https://doi.org/10.1016/0012-8252\(76\)90052-0](https://doi.org/10.1016/0012-8252(76)90052-0)

Sun SS, McDonough WF. 1989. Chemical and isotopic systematics of oceanic basalts: implications for mantle composition and processes. Geological Society, London, Special Publications. 42(1):313–345. <https://doi.org/10.1144/GSL.SP.1989.042.01.19>

Trettin HP, editor. 1991. *Geology of the Innuitian Orogen and Arctic Platform of Canada and Greenland* [Internet]. Ottawa, Canada K1A 0S9: Geological Society of America; [accessed 2024 Jun 10]. <https://doi.org/10.1130/DNAG-GNA-E>

Trettin HP. 1996. *Geology - Parts of Cape Stallworthy and Bukken Fiord*.

Trettin HP, Gabites J, Norford B. 1998. *Pre-Carboniferous Geology of the Northern Part of the Arctic Islands, Northern Heiberg Fold Belt, Clements Markham Fold Belt, and Pearya, Northern Axel Heiberg and Ellesmere Islands*. [place unknown]: Natural Resources Canada, Geological Survey of Canada.

Warr LN. 2021. IMA–CNMNC approved mineral symbols. *Mineralogical Magazine*. 85(3):291–320. <https://doi.org/10.1180/mgm.2021.43>

Whitney D, Evans B. 2010. Abbreviations for Names of Rock-Forming Minerals. *American Mineralogist*. 95:185–187. <https://doi.org/10.2138/am.2010.3371>

Wilson M. 1989. Relation of present-day magmatism to global tectonic processes. In: Wilson M, editor. *Igneous Petrogenesis* [Internet]. Dordrecht: Springer Netherlands; p. 3–12. [https://doi.org/10.1007/978-94-010-9388-0\\_1](https://doi.org/10.1007/978-94-010-9388-0_1)

Winchester JA, Floyd PA. 1977. Geochemical discrimination of different magma series and their differentiation products using immobile elements. *Chemical Geology*. 20:325–343. [https://doi.org/10.1016/0009-2541\(77\)90057-2](https://doi.org/10.1016/0009-2541(77)90057-2)

Winter JD. 2014. *Principles of igneous and metamorphic petrology*. Harlow: Pearson.

Xia L, Li X. 2019. Basalt geochemistry as a diagnostic indicator of tectonic setting. *Gondwana Research*. 65:43–67. <https://doi.org/10.1016/j.gr.2018.08.006>

## Appendix A – Abbreviations

*Table 1: Mineral Abbreviations<sup>1</sup>.*

<b>Name</b>	<b>Abbreviation</b>
Biotite	Bt
Calcite	Cal
Chlorite	Chl
Clinopyroxene	Cpx
Epidote	Ep
K-feldspar	Kfs
Olivine	Ol
Opaque	Opq
Plagioclase	Pl
Quartz	Qz
Amphibole	Amp

---

*1- according to the International Mineralogical Association (IMA) Commission on New Minerals, Nomenclature and Classification (CNMNC) standard (Warr 2021). Opaque lacked an IMA-CNMNC standard abbreviation and was therefore taken from (Whitney and Evans 2010).*

## Appendix B – Point counting grid example

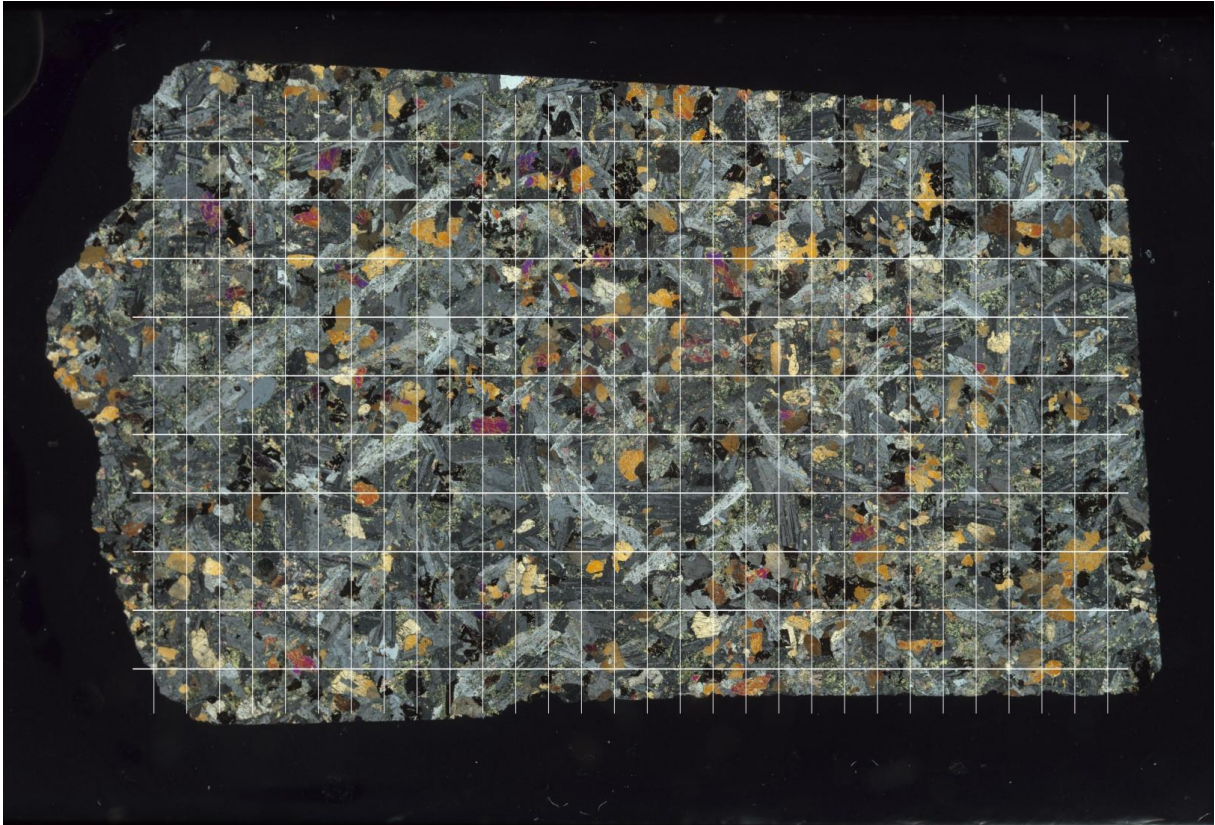


*Figure B1: Figure showing an example of how point counting was conducted, with a grid overlain the thin section. Each mineral at the grid's intersection was counted, totalling 300 minerals.*

## Appendix C – Point counting results

	U c o r n O k p g t c n C o q w p v		R g t e g p v c i U v c p f c g t t q t	
<b>XR3 06 3</b>	Pl	179	59.67	5.66
	Cpx	63	21.00	4.70
	Chl	28	9.33	3.36
	Ol	0	0.00	0.00
	Bt	0	0.00	0.00
	Kfs	0	0.00	0.00
	Qz	0	0.00	0.00
	Cal	0	0.00	0.00
	Ep	24	8.00	3.13
	Opq	6	2.00	1.62
<b>XR3 06 5</b>	Pl	176	58.67	5.69
	Cpx	70	23.33	4.88
	Chl	24	8.00	3.13
	Ol	0	0.00	0.00
	Bt	0	0.00	0.00
	Kfs	0	0.00	0.00
	Qz	0	0.00	0.00
	Cal	0	0.00	0.00
	Ep	20	6.67	2.88
	Opq	10	3.33	2.07

*Continuation of Appendix C*

<b>XR3 96 6</b>	<b>R n</b>	<b>3 7 4</b>	<b>7 2 0 8 9</b>	<b>7 0 9 9</b>
	Cpx	62	20.67	4.68
	Chl	29	9.67	3.41
	Ol	1	0.33	0.67
	Bt	9	3.00	1.97
	Kfs	0	0.00	0.00
	Qz	0	0.00	0.00
	Cal	2	0.67	0.94
	Ep	15	5.00	2.52
	Opq	30	10.00	3.46
<b>XR3 97 3</b>	Pl	171	57.00	5.72
	Cpx	38	12.67	3.84
	Chl	59	19.67	4.59
	Ol	8	2.67	1.86
	Bt	2	0.67	0.94
	Kfs	0	0.00	0.00
	Qz	0	0.00	0.00
	Cal	3	1.00	1.15
	Ep	0	0.00	0.00
	Opq	19	6.33	2.81

*Continuation of Appendix C*

<b>XR3 97 4</b>	<b>R n</b>	<b>3 8 2</b>	<b>7 5 0 5 5</b>	<b>7 0 9 8</b>
	Cpx	54	18.00	4.44
	Chl	54	18.00	4.44
	Ol	3	1.00	1.15
	Bt	0	0.00	0.00
	Kfs	0	0.00	0.00
	Qz	0	0.00	0.00
	Cal	0	0.00	0.00
	Ep	7	2.33	1.74
	Opq	22	7.33	3.01
<b>XR3 97 5</b>	Pl	142	47.33	5.77
	Cpx	0	0.00	0.00
	Chl	19	6.33	2.81
	Ol	0	0.00	0.00
	Bt	0	0.00	0.00
	Kfs	31	10.33	3.51
	Qz	108	36.00	5.54
	Cal	0	0.00	0.00
	Ep	0	0.00	0.00
	Opq	0	0.00	0.00

*Continuation of Appendix C*

<b>XR3 97 7</b>	<b>R n</b>	<b>3 §</b>	<b>7 8 6</b>	<b>7 6 9</b>
	Cpx	87	29.00	5.24
	Chl	14	4.67	2.44
	Ol	0	0.00	0.00
	Bt	0	0.00	0.00
	Kfs	0	0.00	0.00
	Qz	1	0.33	0.67
	Cal	5	1.67	1.48
	Ep	12	4.00	2.26
	Opq	13	4.33	2.35
<b>XR3 97 8</b>	Pl	152	50.67	5.77
	Cpx	69	23.00	4.86
	Chl	37	12.33	3.80
	Ol	0	0.00	0.00
	Bt	1	0.33	0.67
	Kfs	0	0.00	0.00
	Qz	6	2.00	1.62
	Cal	0	0.00	0.00
	Ep	13	4.33	2.35
	Opq	22	7.33	3.01

*Continuation of Appendix C*

<b>XR3 97 9</b>	<b>R n</b>	<b>3 8</b>	<b>7 7 0 8 9</b>	<b>7 6 9</b>
	Cpx	58	19.33	4.56
	Chl	54	18.00	4.44
	Ol	7	2.33	1.74
	Bt	0	0.00	0.00
	Kfs	0	0.00	0.00
	Qz	0	0.00	0.00
	Cal	0	0.00	0.00
	Ep	5	1.67	1.48
	Opq	8	2.67	1.86
<b>XR3 97 ;</b>	Pl	146	48.67	5.77
	Cpx	45	15.00	4.12
	Chl	72	24.00	4.93
	Ol	1	0.33	0.67
	Bt	0	0.00	0.00
	Kfs	0	2.33	0.00
	Qz	0	0.00	0.00
	Cal	1	0.33	0.67
	Ep	14	4.67	2.44
	Opq	21	7.00	2.95

## **Appendix D – Petrographic Analysis**

### ***VP17-41***

The hand sample is an intermediate to coarse-grained mafic rock comprised of alternating green-tinted dark and light grey plagioclase and beige-white plagioclase phenocrysts varying from 2-6 mm, the colour variation probably being due to the phenocrysts experiencing different degrees of weathering. Small amounts of dark green lustrous pyroxene exist on the edges. The lower short side has been weathered. Fluid inclusions can be observed on the backside.

The thin section is medium to coarse-grained with phenocrysts and the primary minerals are plagioclase, clinopyroxene, and epidote, with chlorite and opaques as accessory minerals. The plagioclase grains, identified through their twinning and alteration, vary in size from fine-grained to megacrysts. The fine to coarse-grained plagioclase grains are generally euhedral and tabular, while the megacrysts exist both as anhedral and euhedral grains. The megacrysts are all heavily altered by saussurite with epidote being the primary identified alteration mineral, while the smaller crystals range from light to heavy alteration. The clinopyroxenes are identified through their birefringence, second-order interference colours, cleavage, inclined extinction angle and habit. The grain's habit varies from anhedral to euhedral. On some grains, uralitization to amphibole can be spotted on the rims. Chlorite can be seen with its fibrous habit and green pleochroism and appears blue on cross-polarized light. It seems to be a product of either amphibole or pyroxene alteration, although it is hard to determine. The opaque minerals are most likely hematite based on some of them having a red rim, and they're often found in contact with chlorite. Weathering products can be seen on the left and rightmost sides of the thin section scan.

### ***VP17-43***

The hand sample is an intermediate to coarse-grained mafic rock comprised of alternating green-tinted dark and light grey plagioclase as well as weathered beige-white plagioclase phenocrysts. The phenocrysts vary from 2-8mm on the long side. Small amounts of dark green lustrous pyroxene on the edges. Minuscule amounts of weathering can be observed on the bottom short side.

The thin section is medium to coarse-grained with phenocrysts and the primary minerals are plagioclase and clinopyroxene, with epidote, chlorite and opaques as accessory minerals. The plagioclase grains, identified through their twinning and alteration, vary in size from fine-

grained to megacrysts. The fine to coarse-grained plagioclase grains are generally euhedral and tabular, while the megacrysts exist both as anhedral and euhedral grains. The megacrysts are all heavily altered by saussurite with epidote being the primary identified alteration mineral, while the smaller crystals range from light to heavy alteration. The clinopyroxenes are identified through their birefringence, second-order interference colours, cleavage, inclined extinction angle and habit. The grain habit varies from anhedral to euhedral and is typically sub-rounded, but a few are tabular. On some grains, uralitization to amphibole can be spotted on the rims. Chlorite can be seen with its fibrous habit and green pleochroism and appears blue on cross-polarized light. It seems to be a product of either amphibole or pyroxene alteration, although it is hard to determine. The opaque minerals are most likely hematite based on some of them having a red rim, and they're often found in contact with chlorite. Tiny flakes of weathering products can be seen on the centre-rightmost side of the thin section scan.

#### ***VP17-44***

The hand sample is an intermediate to coarse-grained mafic rock comprised of alternating green-tinted dark and light grey plagioclase and a small number of chlorite grains. Small amounts of dark green lustrous pyroxene on the edges. moderate amounts of weathering can be observed on the left long side. Fluid inclusions can be seen on the backside.

The thin section is medium to coarse-grained with phenocrysts and the primary minerals are plagioclase, clinopyroxene, and opaques, with epidote, chlorite, olivine, calcite and biotite as accessory minerals. The plagioclase grains, identified through their twinning and alteration, vary in size, generally being coarse-grained but with one grain being a megacryst. The plagioclase grains are generally tabular but vary from anhedral to euhedral. Their degree of alteration varies from low to high, and the megacryst is heavily altered by saussurite with epidote being the primary identified alteration mineral, The clinopyroxenes are identified through their birefringence, second-order interference colours, cleavage, inclined extinction angle and habit. The grains habit varies from anhedral to euhedral and are typically sub-rounded, but a few are tabular. On some grains, uralitization to amphibole can be spotted on the rims. Chlorite can be identified by its fibrous habit, green pleochroism and interference colour. It's generally fibrous and varies in shape from tabular to elongated. Biotite appears next to chlorite in the samples in the midst of altering to chlorite, identified through its brown pleochroism and interference colour, and micaceous habit. Based on this, the chlorite seems to be a product of biotite and pyroxene alteration. The opaque minerals are most likely hematite

based on some of them having a red rim, and they're often found in contact with chlorite and biotite. The olivine grains are identical to clinopyroxene but are determined to be olivine due to having no cleavage. Calcite appears as singular grains. Weathering products can be seen on the top right side of the thin section scan.

### ***VP17-51***

The hand sample is an intermediate-grained mafic rock comprised of alternating green-tinted dark and light grey plagioclase. Large amounts of dark green lustrous pyroxene on the edges and sides. Fluid inclusions can be observed on the backside.

The thin section is fine to intermediate grained and the primary minerals are plagioclase, clinopyroxene, and chlorite, with opaques, olivine, K-feldspar, calcite and biotite as accessory minerals. The plagioclase grains, identified through their twinning and alteration, are all uniformly intermediate-grained. They're generally tabular but vary from anhedral to euhedral. Their degree of alteration varies from low to medium, and the saussurite is identified as an epidote in some plagioclase grains. The clinopyroxenes are fine-grained and identified through their birefringence, second-order interference colours, cleavage, inclined extinction angle and habit. The grain's habit varies from anhedral to euhedral and is typically sub-rounded. On some grains, uralitization to amphibole can be spotted on the rims. Chlorite can be identified by its fibrous habit, green pleochroism and blue interference colour. It's generally fibrous and appears in all sorts of shapes. Small amounts of biotite appear next to chlorite in the samples in the midst of altering to chlorite, identified through its brown pleochroism and interference colour, and micaceous habit. Based on this, the chlorite seems to be a product of biotite and pyroxene alteration. The opaque minerals are most likely hematite based on some of them having a red rim, and they're often found in contact with chlorite and biotite. Singular K-feldspar grains were identified from their exsolution lamellae. The olivine grains are identical to clinopyroxene but are determined to be olivine due to having no cleavage. Calcite appears as singular grains.

### ***VP17-52***

The hand sample is an intermediate to coarse-grained mafic rock comprised of alternating green-tinted dark and light grey plagioclase groundmass, and many plagioclase phenocrysts varying from 2-5 mm. Moderate amounts of dark green lustrous pyroxene on the edges and sides. A small amount of weathering on the top short side can be seen. Fluid inclusions can be observed on the backside.

The thin section is fine to coarse with phenocrysts grained and the primary minerals are plagioclase, clinopyroxene, and chlorite, with opaques, olivine and epidote as accessory minerals. The plagioclase grains, identified through their twinning and alteration, vary in size from fine-grained to megacrysts. The fine to coarse-grained plagioclase grains are generally euhedral and tabular, while the megacrysts exist both as anhedral sub-rounded and euhedral tabular grains. The megacrysts are generally lightly altered with saussurite, with epidote being the primary identified alteration mineral, while the smaller crystals range from light to heavy alteration. The megacrysts are also fractured to various degrees. The clinopyroxenes are fine-grained and identified through their birefringence, second-order interference colours, cleavage, inclined extinction angle and habit. The grain habit varies from anhedral to euhedral and is typically sub-rounded. On some grains, uralitization to amphibole can be spotted on the rims. Chlorite can be identified by its fibrous habit, green pleochroism and blue interference colour. It's generally fibrous and appears in all sorts of shapes. The chlorite seems to be a product of pyroxene alteration and perhaps also biotite. The opaque minerals are most likely hematite based on some of them having a red rim, and they're often found in contact with chlorite. The olivine grains are identical to clinopyroxene but are determined to be olivine due to having no cleavage.

### ***VP17-53***

The hand sample is a fine to coarse-grained rock comprised of alternating rounded white quartz and grey plagioclase as well as black-coloured minerals that cannot be identified. The quartz grains are surrounded by a very fine-grained groundmass. Minuscule amounts of weathering on the bottom short side. Fluid inclusions can be observed on the backside.

The thin section is fine to coarse-grained with phenocrysts and the primary minerals are plagioclase, quartz, and K-feldspar, with chlorite and opaques as accessory minerals. The plagioclase grains, identified through their twinning and light alteration, are generally fine to intermediate-grained and anhedral or euhedral. The quartz crystals exist as fine groundmass matrix and also as larger phenocrysts, and are both rounded and tabular. Some quartz crystals also show embayed texture. The k-feldspars were distinguished from quartz and plagioclase by their pleochroism being greyer than quartz as well as exhibiting Carlsbad twinning. Chlorite can be identified with its fibrous habit and green/yellow pleochroism. The mineral that chlorite altered form cannot be identified in the thin section. The opaque minerals are minuscule and cannot be identified.

### ***VP17-55***

The hand sample is an intermediate to coarse-grained dark mafic rock comprised of light grey plagioclase grains. Moderate amounts of dark green lustrous pyroxene on the edges. En echelon striations can be observed. Fluid inclusions can be observed on the backside.

The thin section is fine to intermediate-grained and the primary minerals are plagioclase and clinopyroxene, with chlorite, opaques, calcite and epidote as accessory minerals. The plagioclase grains, identified through their twinning and alteration, are fine to intermediate-grained. They're generally tabular but vary from anhedral to euhedral. Their degree of alteration varies from low to medium, and the saussurite is identified as an epidote in some plagioclase grains. The clinopyroxenes are fine-grained and identified through their birefringence, second-order interference colours, cleavage, inclined extinction angle and habit. The grain habit varies from anhedral to euhedral. On some grains, uralitization to amphibole can be spotted on the rims. Chlorite can be identified by its fibrous habit, green pleochroism and interference colour. It's generally fibrous and appears interstitially in all sorts of shapes. The chlorite grains are shaped the same as the pyroxenes and thus appear to be a product of pyroxene alteration, and may have also been altered from biotite. The opaque minerals are most likely hematite based on some of them having a red rim, and they're often found in contact with chlorite. Calcite appears as singular grains.

### ***VP17-56***

The hand sample is an intermediate to coarse-grained dark mafic rock comprised of green-tinted light-grey plagioclase grains. Some plagioclase phenocrysts are tabular. Moderate amounts of dark green lustrous pyroxene on the edges. Fluid inclusions can be observed on the backside.

The hand sample is fine to coarse-grained and the primary minerals are plagioclase and clinopyroxene, with chlorite, opaques, quartz and epidote as accessory minerals. The plagioclase grains, identified through their twinning and alteration, are fine to coarse-grained. They're generally tabular but vary from anhedral to euhedral. Their degree of alteration varies from low to medium, and the saussurite is identified as an epidote in some plagioclase grains. The clinopyroxenes are fine-grained and identified through their birefringence, second-order interference colours, cleavage, inclined extinction angle and habit. The grain habit varies from anhedral to euhedral. On some grains, uralitization to amphibole can be spotted on the rims.

Chlorite can be identified by its fibrous habit and green pleochroism and interference colour, but also exists as specks throughout the thin section. It's generally fibrous and appears interstitially in all sorts of shapes. The chlorite grains are shaped like the pyroxenes and thus appear to be a product of pyroxene alteration, and may have also been altered from biotite. The quartz grains are fine to intermediate-sized and anhedral to subhedral. The opaque minerals are most likely hematite based on some of them having a red rim, and they're often found in contact with chlorite.

### ***VP17-57***

The hand sample is a medium-grained dark mafic rock comprised of alternating green-tinted dark and light grey plagioclase and chloritized green plagioclase phenocrysts ranging from 2-6 mm. Some plagioclase phenocrysts are tabular. Small amounts of dark green lustrous pyroxene on the edges. Moderate amounts of beige-red weathering on one side. Fluid inclusions can be observed on the backside.

The thin section is fine to coarse-grained with phenocrysts and the primary minerals are plagioclase, clinopyroxene, and chlorite, with opaques, olivine, and epidote as accessory minerals. The plagioclase grains, identified through their twinning and alteration, are fine to coarse grain-sized, with some larger grains bordering on being referred to as megacrysts. They're generally tabular but vary from anhedral to euhedral. Their degree of alteration varies from low to high, with the larger crystals being heavily altered, and the saussurite is identified as an epidote in some plagioclase grains. The clinopyroxenes are fine-grained and identified through their birefringence, second-order interference colours, cleavage, inclined extinction angle and habit. The grains habit varies from anhedral to euhedral and subrounded to tabular. On some grains, uraltization to amphibole can be spotted on the rims. Chlorite can be identified by their fibrous habit and green pleochroism and interference colour, and also exists as specks throughout the thin section. The grains are generally fibrous and appear interstitially in different shapes. The chlorite grains share shape with the pyroxenes and thus appear to be a product of pyroxene alteration, and may have also been altered from biotite. The opaque minerals are most likely hematite based on some of them having a red rim, and they're often found in contact with chlorite. The olivine grains are identical to clinopyroxene but are determined to be olivine due to having no cleavage. Weathering products can be seen covering the top side of the thin section scan.

### ***VP17-59***

The hand sample is an intermediate to coarse-grained dark mafic rock comprised of green-tinted light-grey plagioclase grains. Some plagioclase phenocrysts are tabular. Moderate amounts of dark green lustrous pyroxene on the edges. Fluid inclusions can be observed on the backside.

The thin section is fine to coarse-grained and the primary minerals are plagioclase, clinopyroxene, and chlorite, with opaques, olivine, K-feldspar, calcite, and epidote as accessory minerals. The plagioclase grains, identified through their twinning and alteration, are fine to coarse-grained. They're generally tabular but vary from anhedral to euhedral. Their degree of alteration varies from low to medium, and the saussurite is identified as an epidote in some plagioclase grains. The clinopyroxenes are fine-grained and identified through their birefringence, second-order interference colours, cleavage, inclined extinction angle and habit. The grain habit varies from anhedral to euhedral. On some grains, uralitization to amphibole can be spotted on the rims. Chlorite can be identified by its fibrous habit, green pleochroism and interference colour, and also can be found throughout the thin section as specks. It's generally fibrous and appears interstitially in all sorts of shapes. The chlorite grains are shaped as the pyroxenes and thus appear to be a product of pyroxene alteration, and may have also been altered from biotite. The k-feldspars were distinguished by their Carlsbad twinning as well as containing no alteration product. The olivine grains are identical to clinopyroxene but are determined to be olivine due to having no cleavage. Calcite appears as singular grains. The opaque minerals are most likely hematite based on some of them having a red rim.

## Appendix E – Alteration ratio

Table E1: Calculation of alteration ratio using  $Al_2O_3/Na_2O^I$ . All samples showed a ratio under 10, implying that elements remained immobile.

Sample	Alteration index
VP17-41	5.82
VP17-43	5.54
VP17-44	3.89
VP17-51	4.17
VP17-52	6.45
VP17-53	3.14
VP17-55	4.82
VP17-56	3.92
VP17-57	5.21
VP17-59	3.60

*1- From (Spitz and Darling 1978).*

## Appendix F – IUGS modal classification

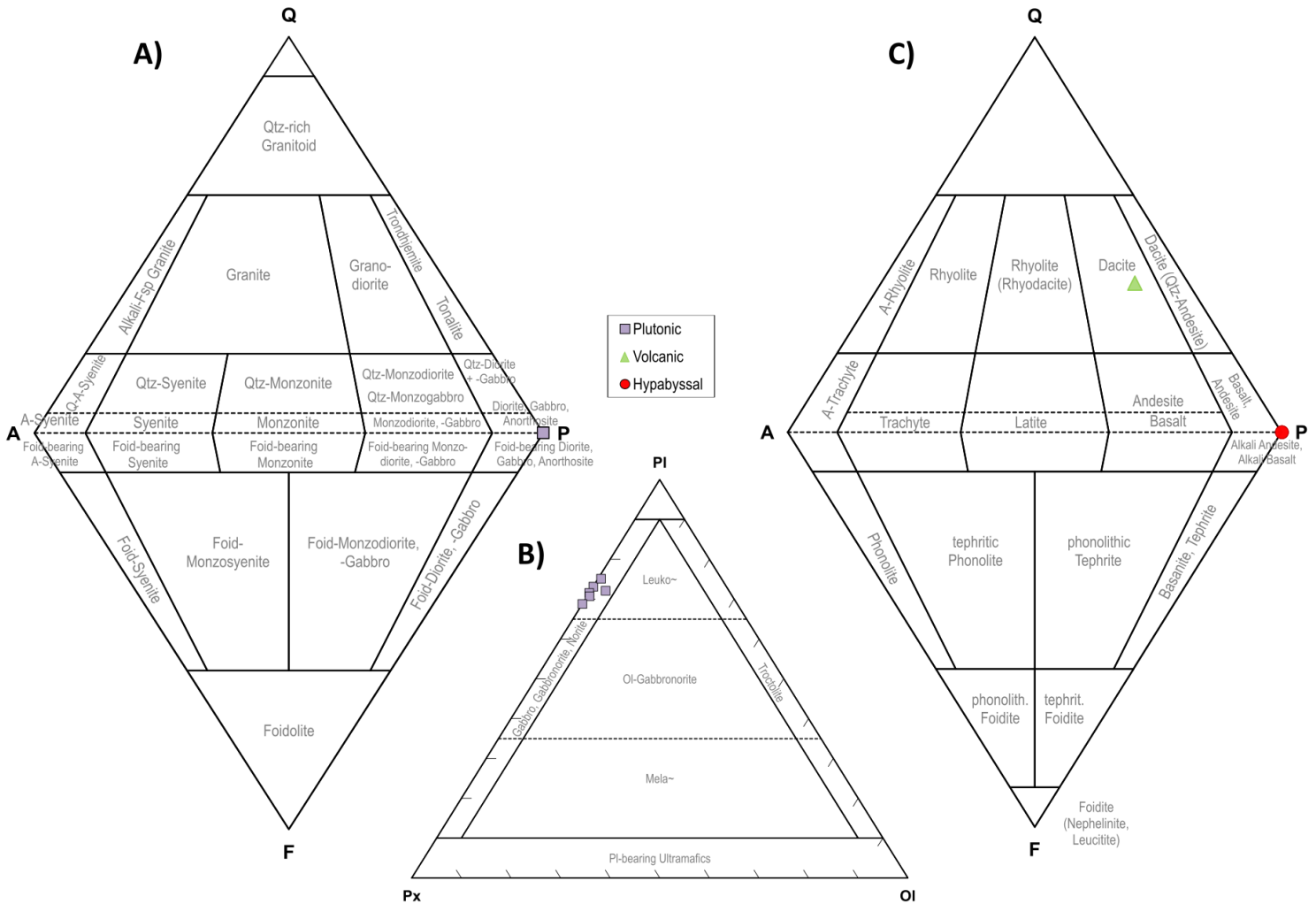


Figure F1: Modal classification of samples using IUGS classification diagrams (Streckeisen 1976). A) QAPF modal classification for plutonic rocks. Plutonic samples classify as gabbros. B) Modal classification of gabbroic rocks based on the proportions of plagioclase, olivine and pyroxene. Gabbros classify as Leucogabbros. C) QAPF modal classification for plutonic rocks. Hypabyssal samples classify as basalt, and volcanic sample as dacite.